Accepted Manuscript

Synsedimentary fault control on the deposition of the Duitschland Formation (South Africa): implications for depositional settings, Paleoproterozoic stratigraphic correlations, and the GOE

Matthew R.Warke, Stefan Schröder

PII: S0301-9268(17)30586-7
DOI: https://doi.org/10.1016/j.precamres.2018.03.001
Reference: PRECAM 5038

To appear in: *Precambrian Research*

Received Date: 23 October 2017
Revised Date: 26 February 2018
Accepted Date: 4 March 2018

Please cite this article as: M. R.Warke, S. Schröder, Synsedimentary fault control on the deposition of the Duitschland Formation (South Africa): implications for depositional settings, Paleoproterozoic stratigraphic correlations, and the GOE, *Precambrian Research* (2018), doi: https://doi.org/10.1016/j.precamres.2018.03.001

This is a PDF file of an unedited manuscript that has been accepted for publication. As a service to our customers we are providing this early version of the manuscript. The manuscript will undergo copyediting, typesetting, and review of the resulting proof before it is published in its final form. Please note that during the production process errors may be discovered which could affect the content, and all legal disclaimers that apply to the journal pertain.

ACCEPTED MANUSCRIPT

Synsedimentary fault control on the deposition of the Duitschland Formation (South Africa): implications for depositional settings, Paleoproterozoic stratigraphic correlations, and the GOE

Matthew R.Warke[1,2*] and Stefan Schröder[1]

[1]*Basin Studies and Petroleum Geoscience, School of Earth and Environmental Sciences, University of Manchester, Manchester M13 9PL, United Kingdom*

[2]*School of Earth and Environmental Sciences, University of St Andrews, St Andrews KY16 9AL, United Kingdom; *mw438@st-andrews.ac.uk*

The Paleoproterozoic Great Oxidation Event (GOE) marks the first significant oxidation of atmosphere and surface environments, and is causally associated with the global disappearance of mass-independent sulfur isotope fractionation (MIF-S). However, fundamental sedimentary aspects of sedimentary successions recording this event (e.g. depositional environment, tectonic setting and stratigraphic correlation) are poorly constrained and often debated, restricting full understanding of causes and effects related to the GOE. In South Africa, MIF-S disappears across the 'mid-Duitschland unconformity' (MDU) in the Duitschland Formation (Transvaal Supergroup). New sedimentological observations of the lower Duitschland Formation have identified up to 5 times thicker and more diverse chert-pebble conglomerates than previously documented. New facies observed include lenticular conglomerates which incise cross-bedded dolomites, and imbricated conglomerates. The overlying MDU is angular in nature, recording an ~15° N dip of the lower Duitschland strata; elsewhere it possesses a disconformable geometry. A new depositional model is proposed where shallow-marine carbonate (ramp) deposition interfaced with wave-influenced Gilbert-type fan deltas in an isolated depocentre produced during synsedimentary faulting. There is no evidence that the MDU formed due to direct glaciation as proposed previously, however glacio-eustatic changes may have had an influence. This study supports lithostratigraphic correlations between the Duitschland and Rooihoogte formations which both register the MIF-S

ACCEPTED MANUSCRIPT

disappearance, but are considered separate lithostratigraphic units, which implies oscillations in MIF-S. The correlation proposed in this study implies a unique MIF-S signal and has important consequences for differentiating true spatiotemporal oscillations in MIF-S chemistry from artificial variations caused by unresolved stratigraphic relations.

1. Introduction

During the 'Great Oxidation Event' ('GOE'; Holland, 2002; 2006) concentrations of atmospheric oxygen are thought to have risen by several orders of magnitude, as documented by the geochemical archive of late Neoarchean to early Paleoproterozoic sedimentary successions from around the world (Bekker et al., 2004; Kump, 2008; Lyons et al., 2014). This rise in oxygen eventually led to the establishment of an ozone layer and homogenization of atmospheric sulfate aerosols, two processes which acted in concert to erase the signature of mass-independently fractionated sulfur (MIF-S) isotopes from the rock record (Farquhar et al., 2000; 2007). This critical change in the sulfur cycle is one of the few points in the GOE at which atmospheric oxygen concentrations can be approximately quantified (at least 10^{-5} present atmospheric levels; Pavlov and Kasting, 2002) and it appears to represent to a discrete temporal event. As such, it has been proposed that disappearance of the MIF-S signal can be utilized as a global, chemostratigraphic correlation surface (Papineau et al., 2007; Hoffman, 2013).

Only two Paleoproterozoic successions preserve the disappearance of the MIF-S signal: the Huronian Supergroup in North America (Papineau et al., 2007) and the Transvaal Supergroup in southern Africa (Guo et al., 2009; Luo et al., 2016). In the case of the latter the disappearance of the MIF-S signal occurs across a prominent intra-formational unconformity within the Duitschland Formation (eastern Transvaal Basin), herein referred to as the mid-Duitschland unconformity, or 'MDU' (Figure 1; Guo et al., 2009; Hoffman, 2013). The MIF-S signal also disappears within the Rooihoogte Formation in the western Transvaal Basin (Luo et al., 2016). The Rooihoogte Formation is commonly correlated with the Duitschland Formation

ACCEPTED MANUSCRIPT

(Coetzee, 2001; Luo et al., 2016) although elsewhere that correlation is rejected (Catuneanu and Eriksson, 2002; Gumsley et al., 2017). This discrepancy has important implications for understanding the evolution of

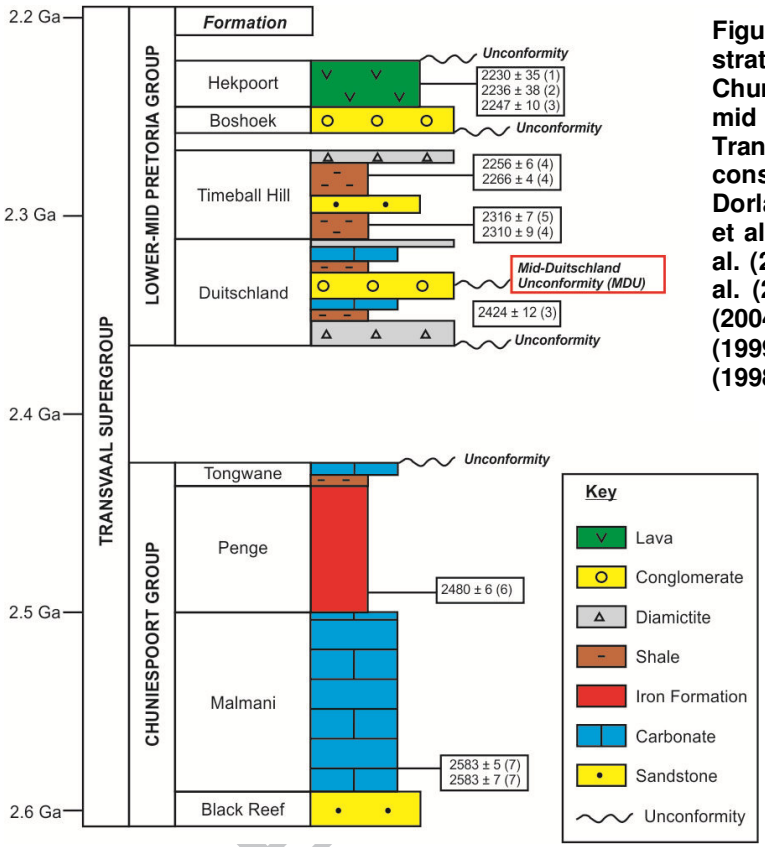

Figure 1: summary stratigraphic column of the Chuniespoort and lower to mid Pretoria groups in the Transvaal Basin. Age constraints from: (1) Dorland (2004), (2) Cornell et al. (1996), (3) Schröder et al. (2016), (4) Rasmussen et al. (2013), (5) Hannah et al. (2004), (6) Nelson et al. (1999), (7) Martin et al. (1998).

atmospheric oxygen. If the two formations are coeval then the disappearance of the MIF-S signal can be viewed as a discrete event, supporting its usage as a chemostratigraphic surface (Hoffman, 2013). In contrast, if the two formations are not correlative it could indicate oscillation between MIF and non-MIF conditions, as proposed by Gumsley et al. (2017).

As such, new lines of sedimentological and stratigraphic evidence need to be provided, which are independent of isotopic trends. Despite its global significance in Paleoproterozoic stratigraphic correlations, sedimentological investigations of the Duitschland Formation are rare and are restricted to unpublished studies (e.g. Button, 1973, Coetzee, 2001). Published studies have focused preferentially on the geochemistry of the succession (Bekker et al., 2001; Frauenstein et al., 2009; Guo et al., 2009). Consequently fundamental questions remain unanswered, such as: (i) the depositional environment and tectonic setting (Button, 1973;

ACCEPTED MANUSCRIPT

Martini, 1979; Coetzee et al., 2001; Eriksson et al., 1993; Catuneanu and Eriksson, 2002; Eriksson and Catuneanu, 2004), (ii) the depositional age (Schröder et al., 2016), and (iii) the processes that formed the MDU

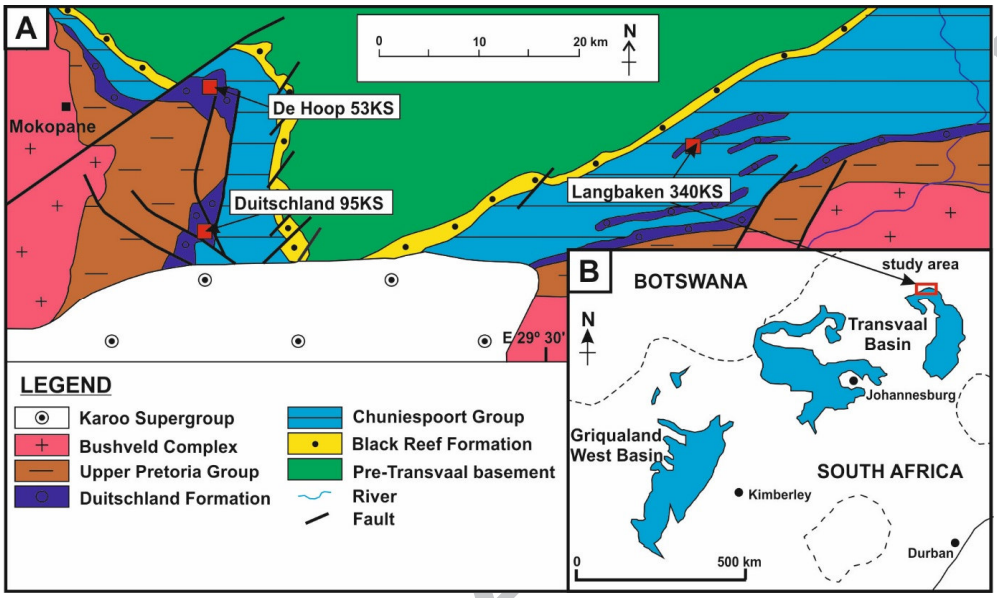

Figure 2: (A) map showing the extent of the Transvaal and Griqualand West basins in South Africa, where the Transvaal Supergroup is preserved; (B) map showing major lithologies in the vicinity of the sudy area (Langbaken 340 KS) and the Duitschland Formation type locality (Duitschland 95KS). Summarised from 1:250 000 geological map, sheet 2428 (Nylstroom) (Geological Survey of South Africa, 1978).

(Hoffman, 2013), and the length of the depositional hiatus it records (Schröder et al., 2016). A robust sedimentological and stratigraphic framework is required in order to fully understand what sedimentary environments and geochemical processes are being recorded in authigenic sediments within the Duitschland Formation (Frauenstein et al., 2009).

This contribution presents the first detailed sedimentological and petrographic study of the Duitschland Formation as exposed on the farm Langbaken 340KS (Figure 2). New sedimentological facies and field relationships are presented which suggest that sedimentation in the Duitschland basin may have been controlled by localized fault movement, possibly in an extensional setting. The model proposed in this contribution holds implications for the nature of the MDU and its application in recently proposed stratigraphic correlation models (Hoffman, 2013). These observations will enable greater comparison with other roughly contemporaneous successions in the Transvaal Supergroup (e.g. Rooihoogte Formation) and further afield.

ACCEPTED MANUSCRIPT

2. Geological Setting

The Duitschland Formation is a mixed sedimentary succession which consists of conglomerates, glacial diamictites, mudstones, marls, siltstones, quartzites, and stromatolitic and non-stromatolitic limestones and dolomites (Figure 3; Coetzee, 2001). The Duitschland Formation is the basal formation of the Pretoria Group of the Transvaal Supergroup (Figure 1). It unconformably overlies both the Tongwane Formation and the Penge Iron Formation due to the widespread erosion and removal (or non-deposition) of the Tongwane Formation prior to Duitschland deposition (Martini, 1979; Schröder and Warke, 2016). It is unconformably overlain by the Timeball Hill Formation in the Duitschland area (Bekker et al., 2001), but further west a conformable contact separates the two formations (Coetzee, 2001; Schröder et al., 2016).

The ~1000 m thick Duitschland Formation is divided into lower and upper parts which are separated by the MDU (Figure 3). The lower Duitschland is composed of a basal chert conglomerate which is overlain by a 30-200 m thick glacial diamictite. Overlying the diamictite are two upward coarsening cycles of mudstone to medium sandstone, with minor limestones, limestone slump breccias, and stromatolitic dolomite deposited during delta progradation (Coetzee, 2001). A prominent chert conglomerate is associated with the MDU; at the type section of Duitschland 95KS ~25 m of chert conglomerate and pebbly quartzite is exposed (Bekker et al., 2001; Coetzee, 2001). Moving upsection from the MDU the upper Duitschland consists of: (i) a coarsening upward (mudstone-quartzite) cycle, (ii) dark grey shale and siltstone, (iii) stromatolitic and oolitic carbonates, (iv) a thin diamictite, (v) an upper stromatolitic brown dolomite, and (vi) a capping dolomite/chert breccia (Coetzee, 2001).

The Duitschland Formation has been variously interpreted as being deposited in a lacustrine (Martini, 1979; Catuneanu and Eriksson, 2002; Eriksson and Catuneanu, 2004), or a shallow marine environment (Button, 1973; Bekker et al., 2001; Coetzee, 2001). The tectonic setting is similarly disputed with foreland basin (Coetzee, 2001; Luo et al., 2016) and rift basin (Eriksson et al., 1991; 1993; 2011; Catuneanu and Eriksson, 1999; 2002; Eriksson and Catuneanu, 2004)

ACCEPTED MANUSCRIPT

settings proposed. The Duitschland Formation has been correlated with the Rooihoogte Formation based on litho-, sequence-, and chemostratigraphic similarities (Coetzee, 2001; Luo et

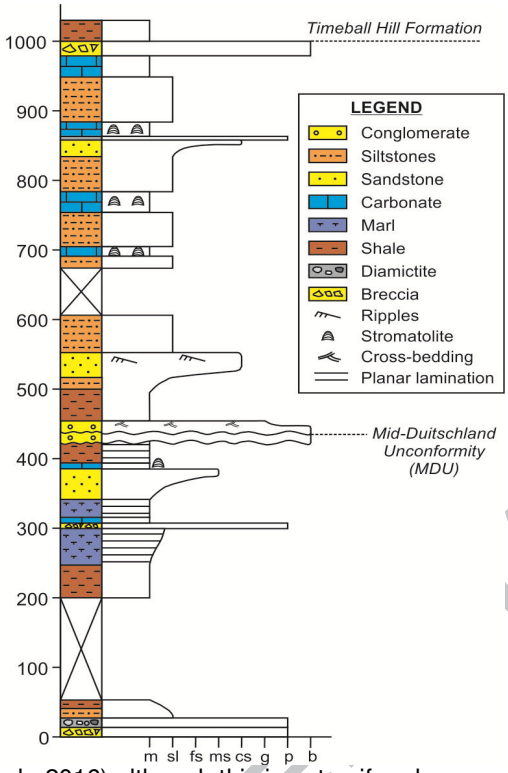

al., 2016) although this is not uniformly accepted (Catuneanu and Eriksson, 2002; Eriksson and Catuneanu, 2004; Gumsley et al., 2017). The c is constrained to between ~2480 and ~2310 Ma ng Penge Iron Formation and the overlying Time l., 1999; Hannah et al., 2004; Rasmussen et al., a maximum depositional age of 2424 ± 12 Ma fc et al., 2016).

Figure 3: summary sedimentary log through the Duitschland Formation as compiled from numerous field localities and core logs by Coetzee (2001). Note ~25 m of conglomerate is associated with the MDU. Throughout this chapter 'lower Duitschland' and 'upper Duitschland' refer to the portions of the succession below and above the MDU respectively.

3. Methods

Mapping at 1:10,000 scale was conducted on the farm Langbaken 340 KS (Figure 4) and four sedimentological logs were measured at 1:50 scale using a 2 m stainless steel Jacob's staff and

ACCEPTED MANUSCRIPT

Abney level. Clast counts were conducted using a 0.5x0.5 m quadrat and the long-axis length (mm), clast roundness and clast lithology were recorded (Tucker, 2003). Petrographic analysis was conducted on 32 polished thin sections and consisted of transmitted and reflected light microscopy and point-counting (n = 300). X-Ray Diffraction (XRD) was used to determine the mineralogical composition of 21 samples using a Bruker D8 Advance Diffractometer (Cu Kα X-

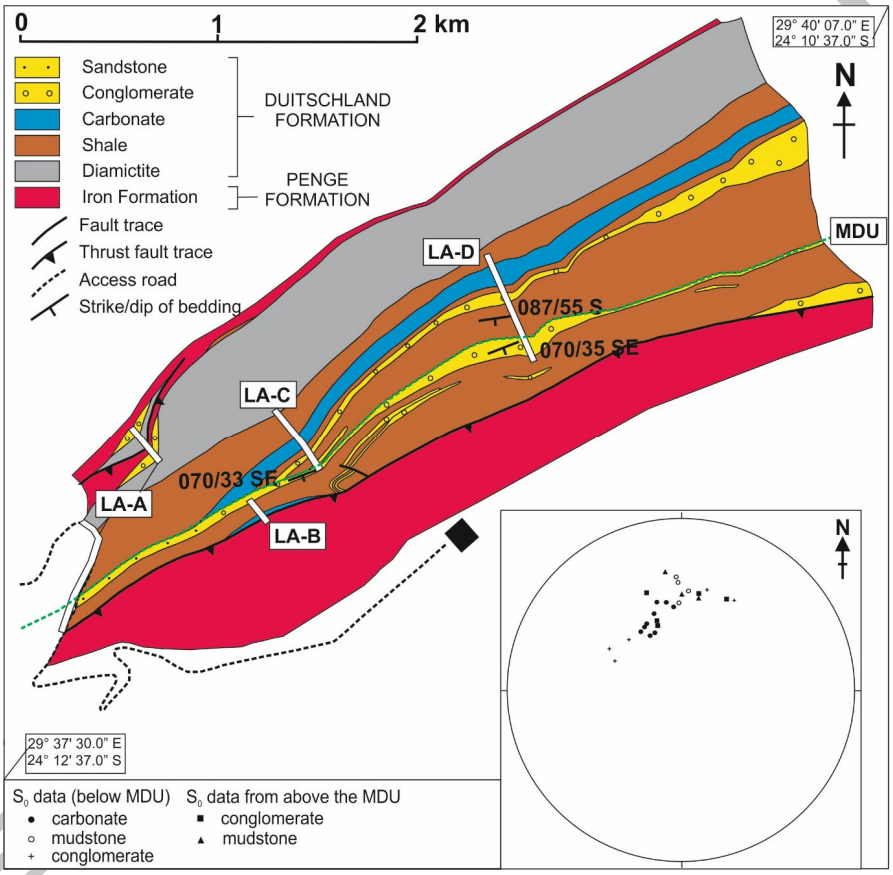

Figure 4: geological map of the farm Langbaken 340KS, showing the position of measured logs (Figure 6). Note that the large apparent thickness of diamictite and the variable thickness of conglomerates units in the east of the study area is due to their preservation on dip slopes with ~150 m of vertical relief.

ray source) at the Williamson Research Centre at the University of Manchester (Table 5.1).

Samples were scanned from 5 to 70° 2θ using a step size of 0.02° and a counting time of 0.2 seconds per step.

4. Results

ACCEPTED MANUSCRIPT

4.1 Mapping and field observations

The Duitschland Formation on the farm Langbaken 340KS is preserved in the footwall of a thrust fault which trends northeast-southwest (~ 060 °) and dips to the south-east (Figure 4); the dip magnitude of the thrust is not well constrained. In the south of the study area most of the upper Duitschland has been removed through thrusting along this fault. The southward dipping trend of the thrust fault is consistent with the Mhlapitsi fold and thrust belt first which formed in response to positive inversion along the Thabazimbi-Murchison Lineament (McCourt, 1995; Button and Cawthorn, 2015). The hanging wall of the fault consists of the Penge Iron Formation, which also outcrops on the north side of the study area where an unconformable (not tectonic) contact is observed. Near to the thrust fault trace (i.e. <50 m) conglomerate clasts show deformation fabrics and in thin-section recrystallized quartzites commonly show undulose extinction. Beds of conglomerate immediately adjacent to the fault contact have been folded into a synformal syncline. The thrust fault contact is commonly associated with irregular, anastomosing silica veining. A small thrust imbricate repeats units in the north-west of the study area (Figure 4). The floor and roof fault contacts of the imbricate are associated with the same style of silica veining noted along the main thrust contact; iron formations within the imbricate are heavily deformed into tight and isoclinal folds. Throughout the remainder of the section no evidence for tectonic deformation is seen.

Mapped units in the study area are predominantly assigned to the lower Duitschland Formation, however significant differences in facies are noted between lower Duitschland facies on Langbaken and those preserved at the type locality; descriptions and interpretations of the mapped lithofacies are described below. The lower and upper parts of the succession are separated by a prominent angular unconformity (Figure 5). The stratigraphic position of this unconformity and its association with the conglomerate facies suggests that it is a local expression of the MDU. Following correction for later tilting associated with positive inversion, the average strike and dip of the bedding beneath the unconformity was calculated as 135/15 NE, confirming that the MDU was angular in nature at Langbaken.

ACCEPTED MANUSCRIPT

4.2 Lithofacies analysis

Sample ID	Log	Height (m)	Lithofacies	Phases identified
LA 1	LA-A	440	LF5C	Quartz, dolomite, kutnahorite, albite, clinochlore
LA 4	LA-A	60	LF6D	Quartz, hematite, goethite, microcline
LA 5	LA-A	115	LF2	Quartz, hematite, goethite
LA 10	LA-A	295	LF3	Quartz, muscovite, kaolinite
LA 15	N/A	N/A	LF5B	Quartz, dolomite, calcite, clinochlore, muscovite
LA 16	N/A	N/A	LF5B	Quartz, dolomite, calcite, clinochlore
LA 17	N/A	N/A	LF3	Quartz, ankerite, hematite, dravite, kaolinite
LA 20	N/A	N/A	LF3	Quartz, clinochlore, muscovite
LA 21	LA-C	43.4	LF5A	Quartz, ankerite, calcite, clinochlore, biotite
LA 22	LA-C	45	LF5B	Quartz, ankerite, calcite, biotite
LA 23	LA-C	50	LF5B	Quartz, dolomite, calcite, clinochlore, biotite
LA 27	LA-C	71	LF4	Quartz, dolomite, calcite, clinochlore, biotite
LA 28	LA-C	118	LF8	Quartz, biotite, goethite
LA 29	LA-C	137	LF7	Quartz, muscovite, kaolinite
LA 30	LA-C	168	LF7/8	Quartz, hematite, muscovite, goethite, kaolinite
LA 31	N/A	N/A	LF8	Quartz, hematite, clinochlore, biotite
LA 32	LA-D	79	LF5A	Quartz, calcite, clinochlore, biotite, grunerite
LA 33	LA-D	78.2	LF5A	Quartz, ankerite, calcite, clinochlore, biotite
LA 34	LA-D	88.5	LF5A	Quartz, dolomite, calcite, clinochlore, biotite
LA 38	LA-D	168.5	LF6C	Quartz, biotite, goethite
LA 40	LA-D	511	LF3	Quartz, hematite, kaolinite

Lithofacies (LF) were identified and correlated between sections (Figure 6), and microfacies and XRD analyses (Table 1) were conducted. Field and petrographic observations of each lithofacies are presented below (summarized in Table 2); interpretations are discussed in following sections.

4.2.1 LF1: Iron formation

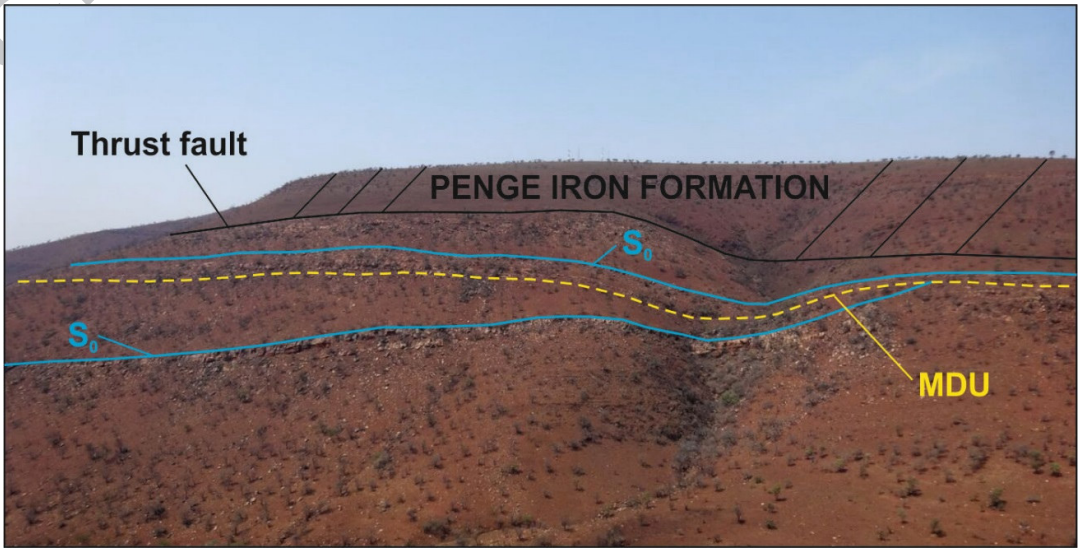

ACCEPTED MANUSCRIPT

Figure 5: photograph showing the angular nature of the MDU at Langbaken 340KS. The MDU is highlighted with a yellow dashed line. Blue lines show the geometry of bedding (S_0) above (average = 087/45 S) and below (average = 068/37 SE) the MDU. The black line marks the thrust fault contact between the Duitschland Formation and the older, but overlying, Penge Iron Formation. Prominent units are conglomerate facies.

ACCEPTED MANUSCRIPT

ACCEPTED MANUSCRIPT

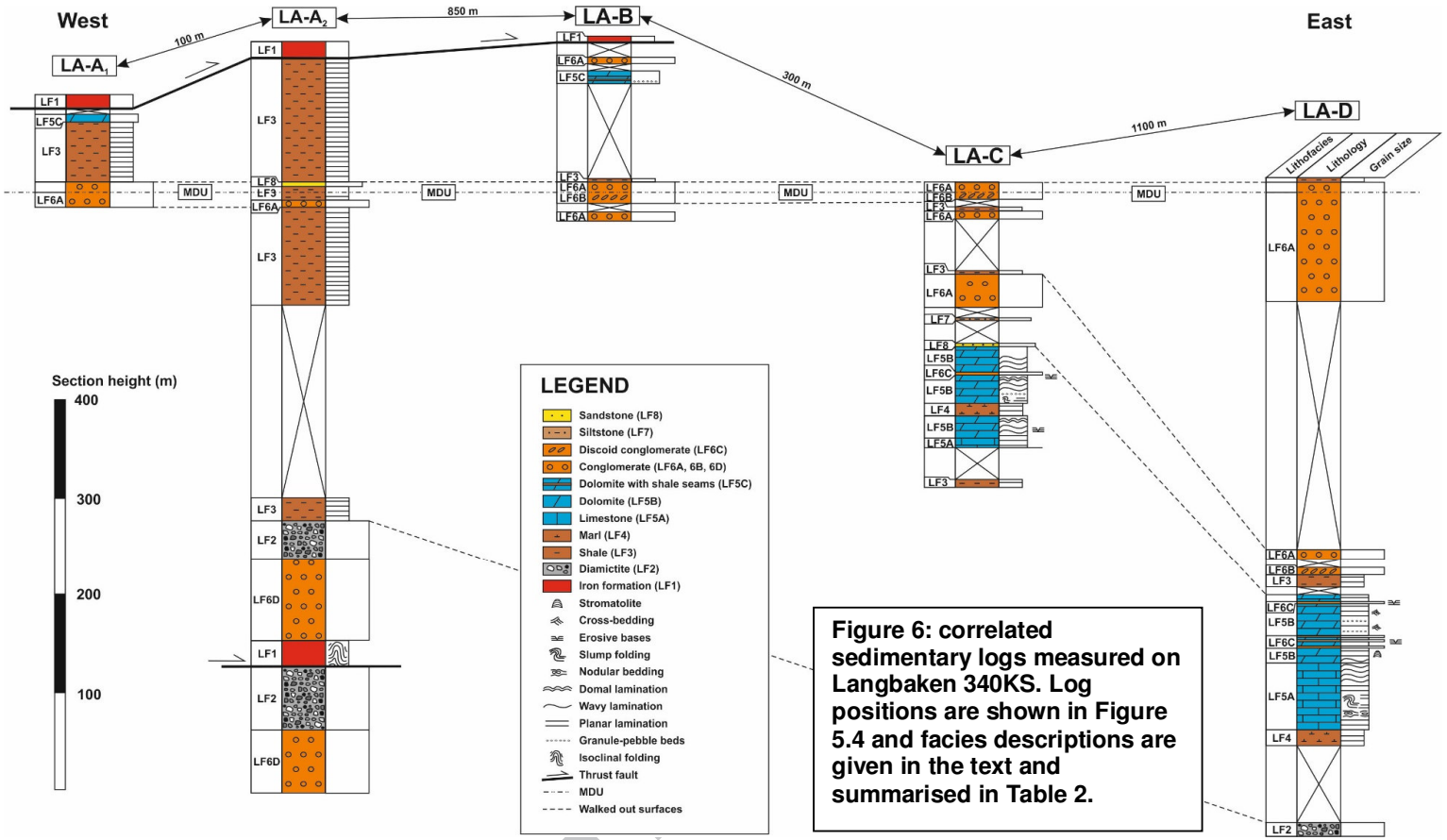

Figure 6: correlated sedimentary logs measured on Langbaken 340KS. Log positions are shown in Figure 5.4 and facies descriptions are given in the text and summarised in Table 2.

Lithofacies	Field Description	Sedimentary structures	Microfacies	Interpretation

ACCEPTED MANUSCRIPT

LF1 –Iron formation	Rusty, brown-red weathering; cm-scale chert laminations	Localised conglomeratic-brecciation textures beneath basal Duitschland unconformity	Alternating mm tick layers of chert and hematite; goethite oxidation common	Exposed and slightly reworked, weathered IF deposited in low energy setting
LF2 - Diamictite	Red-brown weathering, ~30 m thick; massive, matrix supported with clasts of IF, chert and quartz – some striated	Striated clasts, no stratification.	Subrounded to subangular chert clasts in fine grained ferruginous matrix with goethite overprint	Glacial diamictite composed of eroded portions of Penge IF
LF3 – Terrigenous shales	Fissile, brown-weathering with micaceous cleavage planes	Fine lamination	Silt grains within fine kaolinite and goethite rich matrix	Overlying diamictite – low energy, distal depositional setting. With conglomerates – lower energy sedimentation on prodelta and between delta lobes
LF4 - Marls	Mustard yellow weathering calcareous muds with dolomite interbeds	Fine lamination	Carbonate rich and poor bands 3-5 mm thick. Sulphides in association with carbonate veining.	Transitional between shales and lower carbonates – deposited in basin or on outer ramp
LF5A – Lower carbonates (limestones)	Grey-green weathering, medium grey on fresh surface; 11.5-50 m thick	Planar and wavy lamination. Slump folding with axial planes that dip south	Granular recrystallized calcite with minor quartz and sulphides. Stylolites with chlorite and hematite. Biotite overprint	Deposition on a southward dipping palaeoslope without traction current – outer ramp
LF5B – Lower carbonates (dolomites)	Brown-yellow weathering; 14-44.5 m thick	Planar, wavy and domal lamination. Chert granule and pebble beds, incisive lenticular conglomerates. Cross-bedding near top	Granular recrystallized dolomite. Stylolites with pyrite, biotite and chlorite. Minor carbonate veins.	Shallowing upwards to wave base, and interaction with prograding Gilbert delta
LF5C – Upper carbonates (dolomites)	Olive green to brown-yellow weathering; 20.5 m thick and above MDU	Interbedded mm to cm thick mudstone seams with chert granule beds	As LF5B	Similar depositional environment to LF5B, but slightly deeper due to mudstone seams and no cross bedding
LF6A - Conglomerate	Red-cream weathering, clast-supported chert conglomerate; total thickness of 35-114.5 m.	Massive and poorly sorted with mean clast size of 2.2-3.8 cm, but up to cobble-boulder grade seen	Not determined	Gilbert-delta foreset/delta front conglomerates
LF6B- Discoid conglomerate	As LF6A, but discoidal clasts have preferred orientation; 10-13 m thick	Southward (seaward) imbrication of discoidal clasts	Not determined	Gilbert-delta wave-influenced topsets/delta top conglomerates
LF6C – Lenticular conglomerate	Chert granule and pebble beds and lenticular beds of composition LF6A within LF5B	Lenticular bedding with erosive lower contact and dolomite onlapping on upper contact	Granule beds – recrystallized carbonate with chert and other fine-grained lithic clasts	Lenticular conglomerates as debris flows from delta front eroding into bottomsets. Granule beds as settling from buoyant plume generated at subaerial/subaqueous fan interface and transported into basin.
LF6D – Basal conglomerate	As LF6A, but with BIF and carbonate clasts; 65-75 m thick	Erosive upper contact which is overlain by LF2	Chert clasts with matrix of quartz, hematite and goethite, similar to LF2	Possibly glacial outwash, not related to Gilbert delta system.
LF7 - Siltstone	Red-brown weathering with micaceous cleavage planes; 8 m thick	Incised by LF6A	Silt to fine sand clasts within matrix of hematite, goethite, kaolinite and chlorite.	Bottomset or silty topset deposits
LF8 - Sandstone	Pink grey weathering; grade laterally from LF6A beds	None noted	Litharenite to lithic greywacke composition. At thrust fault recrysta-llized with undulose extinction	Foreset and/or topset deposits

Table 2: summarized lithofacies descriptions and interpretations. See text for more detailed discussion.

ACCEPTED MANUSCRIPT

ACCEPTED MANUSCRIPT

Iron formation beds (LF1) consist of cm-scale laminations of dark-grey and white-grey chert which weathers to a distinct rusty, brown-red colour. In thin section chert layers 6-8 mm thick (32.3 %) are interbedded with 1-3 mm thick bands of hematite (39 %) which are commonly oxidized to goethite (28.7 %). Goethite replaces hematite, forming pseudomorphs, but it also occurs as a kinked, fibrous habitat that is nucleated on (and radiates out from) partially altered hematite. Beds of LF1 are exposed in the northern part of the study area where they are unconformably overlain by a massive diamictite bed (LF2, see below) and are intercalated with red-brown micaceous shales. Along the LF1/LF2 contact a matrix supported conglomerate is developed which is composed of sub-rounded to angular clasts of iron-formation set within a fine-grained ferruginous matrix, though in some areas it more closely resembles an angular, clast supported breccia (Figure 7A and B). This facies shows little deformation except in the small imbricate in the north-west where the iron formation has been tightly and isoclinally folded. Beds of LF1 also comprise the hanging wall of the thrust fault in the southern part of the study area.

4.2.2 LF2: Diamictite

The purple-red weathering diamictite unit (LF2) is ~30 m thick and unconformably overlies: (i) red-brown shales, (ii) iron formation, and (iii) conglomerates (LF6D, see below). It exhibits no discernable stratification and is matrix supported with clasts of iron-formation, chert and quartz set within a fine grained ferruginous matrix. Clasts up to 20 cm in length are observed, though average clast size is 2.2 cm (n=152; Table 3); some clasts are striated (Figure 7C). The degree of clast roundness varies: rounded (17.8 %), subrounded (28.3 %), subangular (14.5 %) and angular (39.5 %). In thin section the diamictite consists of subrounded to subangular, mm-scale chert clasts (12.7 %) which are set within a fine grained, ferruginous matrix. The matrix is comprised of quartz (6.7 %), hematite (60.3 %), and goethite (16.7 %). Goethite occurs both as a fine-grained replacement of the ferruginous matrix and as elongate, fibrous crystals which overprint and obscure depositional textures.

4.2.3 LF3: Shales

ACCEPTED MANUSCRIPT

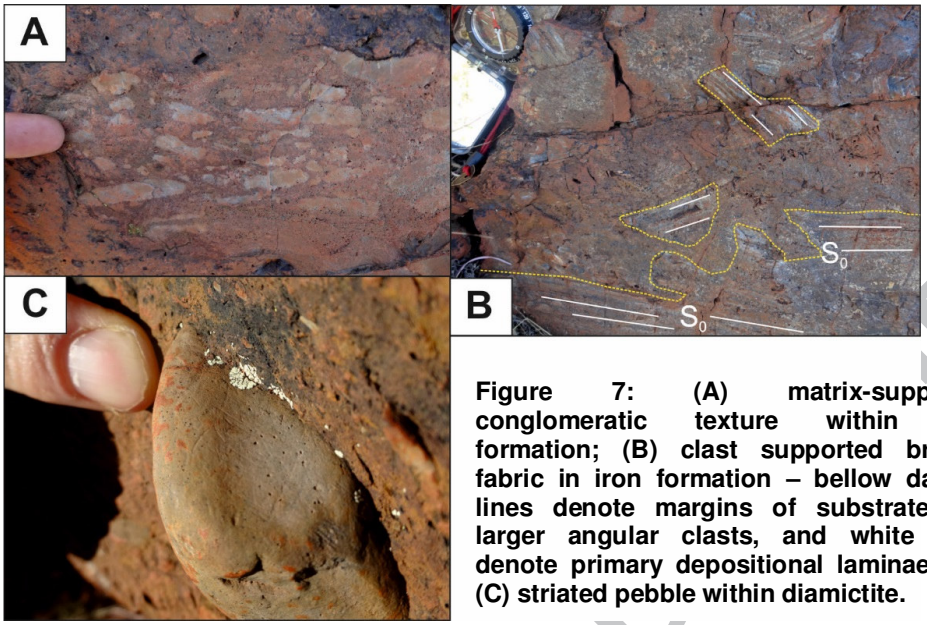

Figure 7: (A) matrix-supported conglomeratic texture within iron formation; (B) clast supported breccia fabric in iron formation – bellow dashed lines denote margins of substrate and larger angular clasts, and white lines denote primary depositional laminae (S_0); (C) striated pebble within diamictite.

Fissile, brown, micaceous shales (LF3) are present at several stratigraphic levels in all logs (Figure 6) and are pervasively weathered and infrequently exposed. Shales are interbedded with conglomerates in the east of the study area (Figure 6). In thin section shale samples have a prominent goethite overprint. In many samples 'halos' of goethite are centred around strongly corroded, anhedral hematite grains, suggesting oxidation during weathering. This facies also contains silt-grade quartz grains within a clay (kaolinite) and goethite-rich matrix. Muscovite is commonly concentrated along cleavage planes.

4.2.4 LF4: Calcareous shales (marls)

Calcareous shales (LF4) are exposed in logs LA-C and LA-D (Figure 6), where they occur within the lower carbonate facies. Though similar to LF3 they are distinguished by discrete layers of carbonate minerals and some mm-thick, mustard-yellow weathering, dolomite interbeds. When viewed under the microscope marl samples are divided into light, carbonate-rich, and dark, carbonate-poor bands which are 3 to 5 mm thick. The dark bands are comprised of silt grade angular to sub-angular grains of quartz and chert, in addition to biotite, clinochlore, and hematite. Dark bands also contain small amounts of 100-200 µm dolomite crystals. Lighter layers contain a higher amount of carbonate material, which is also generally coarser (200-400 µm). The internal

ACCEPTED MANUSCRIPT

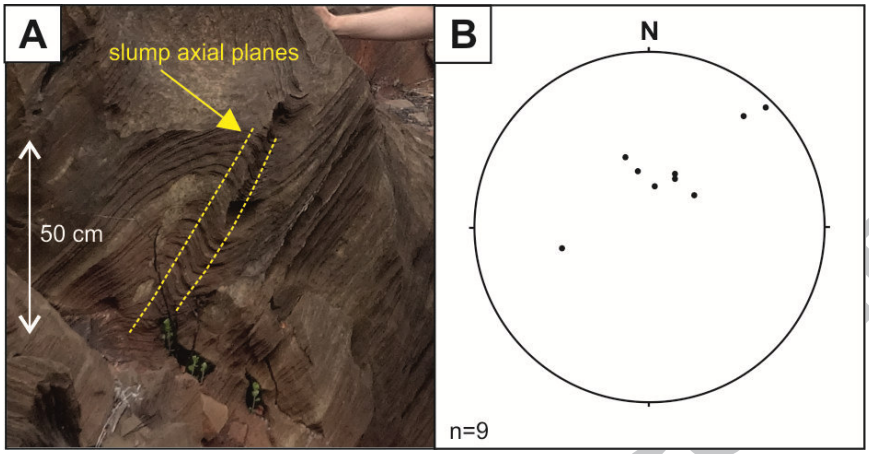

Figure 8 (above): (A) dm scale slump folding noted within limestones of LF5A, with axial planes highlighted; (B) poles to the planes of slump axial planes, corrected for post-depositional tilting. Data are variable (due to nature of slumping process) but suggest a north to south orientated palaeoslope.

lamination around angular chert clasts (up to 2.3 mm long) has been deformed. Pyrite, chalcopyrite and clinochlore are spatially associated with calcite veining.

4.2.5 LF5A: Lower carbonates (limestones)

Grey-green weathering, grey limestone with flat (occasionally wavy) lamination overlie LF4 with a gradational contact. Though predominantly limestone patches and nodules of dolomite are observed. Slump folding is observed in the lower beds (Figure 8A). Measurements made on slump axial planes (n=9) were corrected to remove the dip of bedding above (087/45 S) and below (068/37 SE) the MD unconformity (Figure 8B). Six of the restored axial planes dip southwards by 20-35 °, while two other planes dip south by 72 ° and 85 °, and one dips 42 ° to the north-east (Figure 8B). Five of the eight measured fold axes of slump folds plunge southwest by 3-14 ° and three plunge east-northeast by 4-17 ° (Figure 8B).

Microfacies analysis shows that LF5A is dominated by recrystallized calcite with minor ankerite and dolomite detected using XRD. Average crystal sizes are in the range of 62-181 µm (n=100), however in localized areas coarser crystals, up to 295 µm (n=50), are noted. Coarser crystals

ACCEPTED MANUSCRIPT

display a poikilotopic texture, enclosing smaller crystals of quartz, pyrite and chalcopyrite. Biotite is common throughout and overprints the recrystallized fabric. Bedding sub-parallel stylolites are spatially assocaited with clinochlore and anhedral hematite. Euhedral iron-sulfides (mostly pyrite, minor chalcopyrite) occur throughout, however iron-oxides and chlorite are spatially restricted to the stylolites.

4.2.6 LF5B: Lower carbonates (dolomites)

Wavy-to-planar laminated, brown-yellow dolomite beds (LF5B) overlie the limestones across the study area. Commonly LF5B dolomites are interbedded with granule and pebble beds (Figure 9A,B), and incised by up to four discrete beds of lenticular conglomerates (LF6C; Figure 11C). Near the top of the LF5B beds the wavy lamination forms broad 1-2 m wide domes which are <5 cm in height and may be stromatolitic laminations. In log LA-D dolomites show wavy and domal (stromatolitic) lamination. The dolomite beds are predominantly planar laminated, with the exception of three beds of cross-bedded dolomite (Figure 6). One cross-bedded dolomite bed fines upwards and entrains angular quartz/chert granules at the base of the bed. In thin section textures vary from partially to fully recrystallized carbonates, which are finely crystalline with average crystal sizes of ~30-54 μm (n=400). Stylolites are common and are spatially associated with occurrences of euhedral pyrite, biotite and clinochlore. Rounded, chert clasts (up to 18.7 %) and of millimeter scale, are observed which have encasing silica and carbonate cements. Some samples preserve thin carbonate veins.

4.2.7 LF5C: Upper carbonates with intercalated thin mudstone beds

Exposed above the MGU (log LA-B; Figure 6) this lithofacies consists of 20.5 m of olive-brown to mustard-yellow dolomite, which is a light grey on fresh surfaces. Beds are cm-dm scale in thickness, with a planar to crinkly lamination, and mm-thick seams of intercalated calcareous mudstone. This unit contains admixed quartz granules which are typically 2-40 mm in length and are predominantly angular. These granules constitute ≤ 5-10 % of this facies and are texturally similar to those seen in LF6C. These carbonates consist of recrystallized, non-planar

ACCEPTED MANUSCRIPT

dolomite and exhibit similar microfacies to LF5B. They contain minor amounts of detrital quartz (1.7-3.3 %) and chert clasts (0-3.3 %), in addition to trace amounts of biotite (0-1 %) and pyrite (2 %). There are two populations of pyrite: (i) anhedral pyrite associated with bedding sub-parallel stylolites, and (ii) euhedral pyrite, overprinting the recrystallized texture. Clinochlore is restricted to stylolites. Kutnahorite and albite are detected using XRD, but are not seen in thin-section.

CLAST COUNT	1	2	3	4	5	6
Total clasts counted (n)	162	123	80	172	252	152
Long axis length (%)						
0 < x ≤ 1 cm	19.1	18.7	42.5	47.1	51.6	51.3
1 < x ≤ 5 cm	66.0	60.2	52.5	29.1	37.7	41.4
5 < x ≤ 10 cm	12.4	16.3	3.8	16.9	7.9	5.3
10 < x ≤ 15 cm	2.4	3.3	1.3	3.5	2.7	1.3
15 < x ≤ 20 cm	0	1.6	0	1.2	0	0.7
20 < x ≤ 25 cm	0	0	0	2.3	0	0
Roundness (%)						
Angular	7.5	19.5	7.1	44.0	29.0	39.5
Sub-angular	24.5	21.1	44.7	29.2	25.8	14.5
Sub-rounded	50.0	48.8	42.4	23.2	31.3	28.3
Rounded	17.9	10.6	5.9	3.5	13.8	17.8
Statistics of binned length data						
Estimate of the mean (cm)	3.3	3.8	2.2	3.5	2.3	2.17
Estimate of the variance	5.4	10.2	4.0	20.6	8.4	11.0
Estimate of the standard deviation	2.4	3.2	2.0	4.5	2.9	3.3

Table 3: clast counts 1 and 2 are from conglomerates below the unconformity in the vicinity of logs LA-C and LA-D; clast counts 3 and 4 are from the conglomerates above the unconformity in the vicinity of the logs. Clast count 5 is from the conglomerates above the unconformity in the east of the study area. Clast count 6 was conducted on the diamictite. All values are rounded to one decimal place. All measured clasts were chert.

4.2.8 LF6A: Conglomerates (massive, unstratified)

Massive, clast-supported, chert conglomerates (Figure 9D) outcrop above and below the MDU on Langbaken and vary from 35 to 114.5 m in thickness. Thickness decreases westwards, which correlates with increasing incision of the MDU (Figure 4). Some conglomerate beds are laterally persistent enough to be walked out for over 3 km, while others gradually fine laterally into litharenites (LF8) over distances of 500-900 m. The base of the conglomerate in log LA-C is erosive, cutting down into underlying mudstone and siltstone facies. The matrix of LF6A consists of a mixture of fine-grained quartz, ferruginous mud-grade material, and weathers recessively with a red-cream colour. Five clast counts were conducted on fresh surfaces within

ACCEPTED MANUSCRIPT

the conglomerate to test for any quantifiable differences in clast composition, size and texture between (and within) the conglomerates above and below the unconformity (Table 3). Results show no significant difference in the mean clast size, which varies from 2.2 to 3.8 cm, indicating

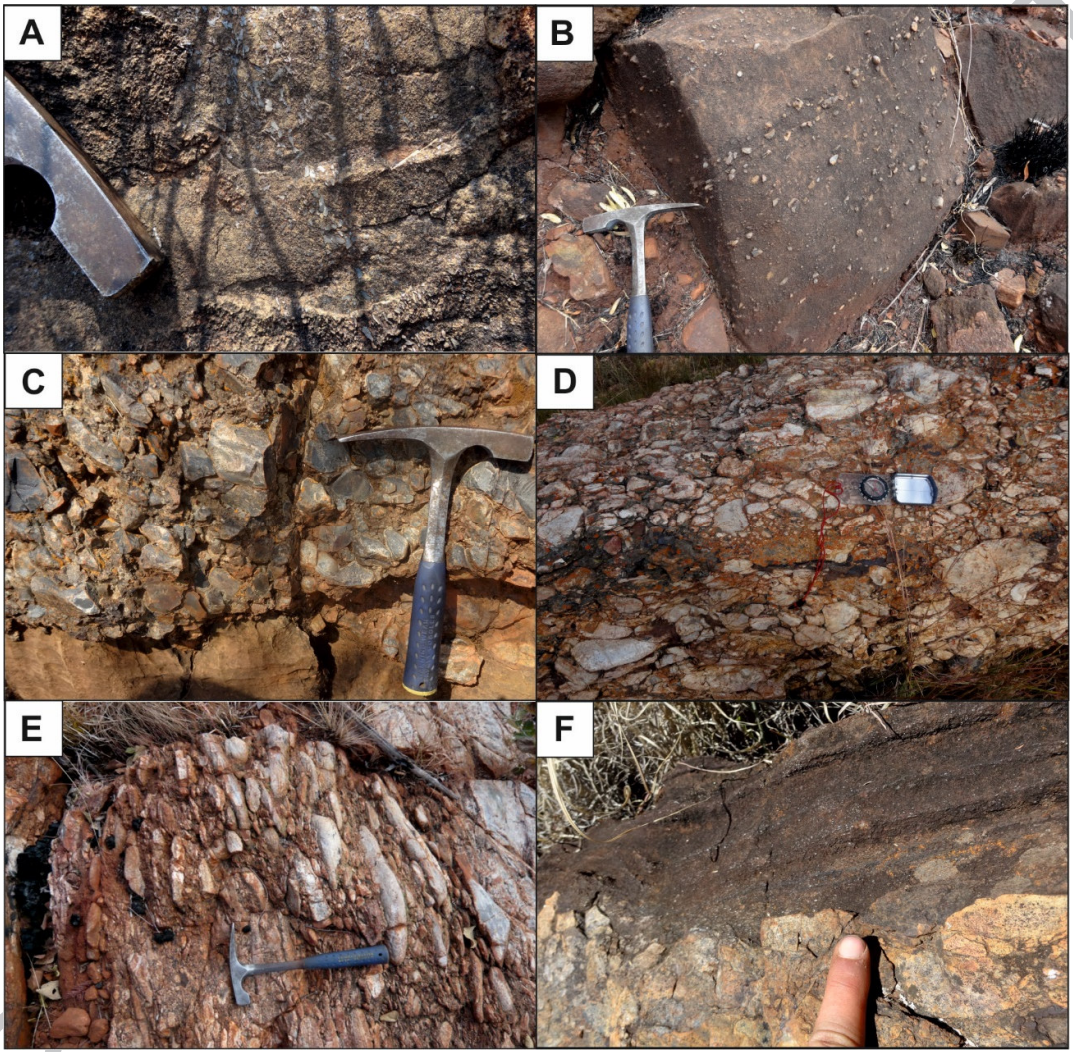

Figure 9: (A) thin chert granule beds within dolomite; (B) chert pebble beds within dolomite; (C) lower surface of lenticular chert conglomerate (LF6C) incising into underlying dolomite; (D) massive chert conglomerate (LF6A); (E) discoid conglomerate (LF6B) with preferentially orientated clast dip direction; (F) planar laminated dolomite draping and onlapping onto upper surface of lenticular conglomerates.

that the conglomerate is gravel dominated despite large (~10 cm long), visually striking, clasts which appear to dominate the poorly sorted, massive fabric. All measured clasts were chert, no other lithologies were noted. Clasts >10 cm were rare (≤3.5 %), and rounded clasts were the least common (3.5-17.9 %). The massive conglomerates beneath the unconformity are slightly

ACCEPTED MANUSCRIPT

more rounded in general (59.4-67.9 % sub-rounded and rounded), whereas the conglomerates above the unconformity tend to be more angular (51.8-73.2 % sub-angular and angular).

4.2.9 LF6B: Discoid conglomerate

The 'discoid' conglomerate is compositionally and texturally similar to the massive conglomerate (LF6A), but is dominated by large, dm-length clasts which have a flatter profile and a preferred southward dip (Figure 9E; Figure 10). Beds of the disc conglomerate are identified in logs LA-B (17.5-30 m), LA-C (229-240 m), and LA-D (190-200 m and 408-418 m); beds are ~10-13 m thick with no internal bedding.

4.2.10 LF6C: Conglomerates (granule-pebble beds and lenticular conglomerates)

Within the lower dolomitic carbonates (LF5B) thin beds of angular chert and quartz granules become gradually more frequent (with higher densities of granules in each bed), and coarsen upwards to beds of pebble-grade, rounded to sub-rounded, chert clasts, resembling the clasts observed in LF6A. In thin section the granule-pebble beds are dominated by a recrystallized, non-planar dolomite matrix (80.0 %) with in which two types of clast occur: (i) angular to sub-angular chert clasts (14.0 %) up to 1.3 mm in length, and (ii) sub-angular to sub-rounded, fine-grained, grey-brown, shale clasts (5.3 %) up to 1.1 mm in length. These pebble beds are succeeded by 1-1.5 m thick lenticular beds of conglomerate which also occur within the dolomite, above the stratigraphic level of the pebble beds. Each lenticular bed has an erosive lower contact which cross-cuts lamination within the dolomite and a bedding parallel upper surface which is onlapped by finely laminated dolomite (Figure 11). The best exposed lenticular bed is 10.5 m wide and 1.5 m thick at the thalweg. The composition and the texture of the conglomerate is the same as that noted in LF6A, although there are fewer cobble-sized clasts; no carbonate clasts were observed.

4.2.11 LF6D: Lower conglomerate

ACCEPTED MANUSCRIPT

Clast-supported, red-brown weathering conglomerate (LF6D) is exposed beneath the diamictite and localized to the north-west of the study area. This conglomerate consists of sub-rounded to sub-angular chert, BIF, and carbonate clasts within a fine-grained, ferruginous matrix; the lower contact with the iron formation is not exposed. The upper contact with the diamictite (LF2) is irregular, possibly erosive. In thin section this unit is similar to the microfacies of LF2 and consists of sub-rounded to sub-angular chert clasts (3 %) up to 4 mm in diameter occur within a ferruginous matrix composed of very fine grained quartz (2 I textures are obscured by a fabric destructive goeth

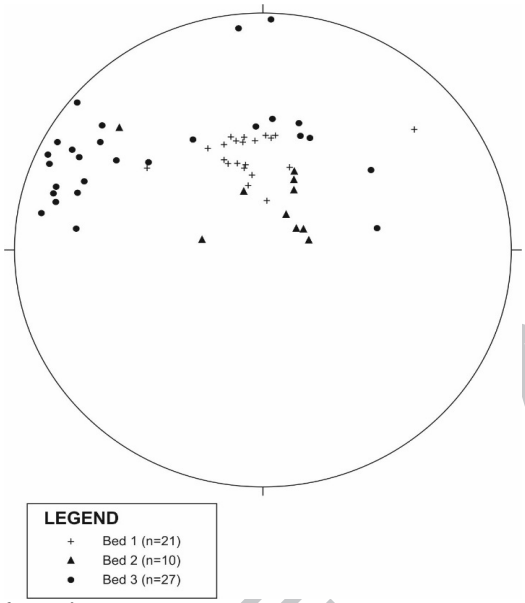

Figure 10: stereogram showing the poles to the dip planes of preferentially orientated discoidal clasts within the discoid conglomerate, corrected to remove the tilt of bedding. While dips are variable, a persistent southward (basinward) dip is seen in all beds.

4.2.12 LF7: Siltstones

Red-brown weathering, micaceous, planar-laminated siltstones (LF7) are exposed beneath, and incised by LF6A conglomerates. Coarse silt to fine-sand grade, poorly sorted, angular to sub-angular chert (29.0 %) and quartz (7.3 %) grains constitute LF7, along with a hematite and goethite dominated matrix (53 %) that contains kaolinite (1 %), clinochlore (8.7 %) and trace amounts of muscovite and pyrite. Quartz cements are developed on the rims of some clasts.

ACCEPTED MANUSCRIPT

4.2.13 LF8: Sandstones

Fine-grained sandstone (LF8) is limited to ~1-2 m thick, pink-grey weathering, beds that grade laterally from conglomerate beds in the west of the study area; these relationships can be walked out for 1-3 km. Sandstone facies range between litharenite and lithic greywacke compositions based on relative matrix content. Lithic greywackes, containing >15 % matrix, occur in the lower section beneath the main conglomerate, whereas litharenites grade laterally into conglomerate beds. All sandstones commonly show little or no feldspar (<2 %), a relatively high proportion of

ACCEPTED MANUSCRIPT

ACCEPTED MANUSCRIPT

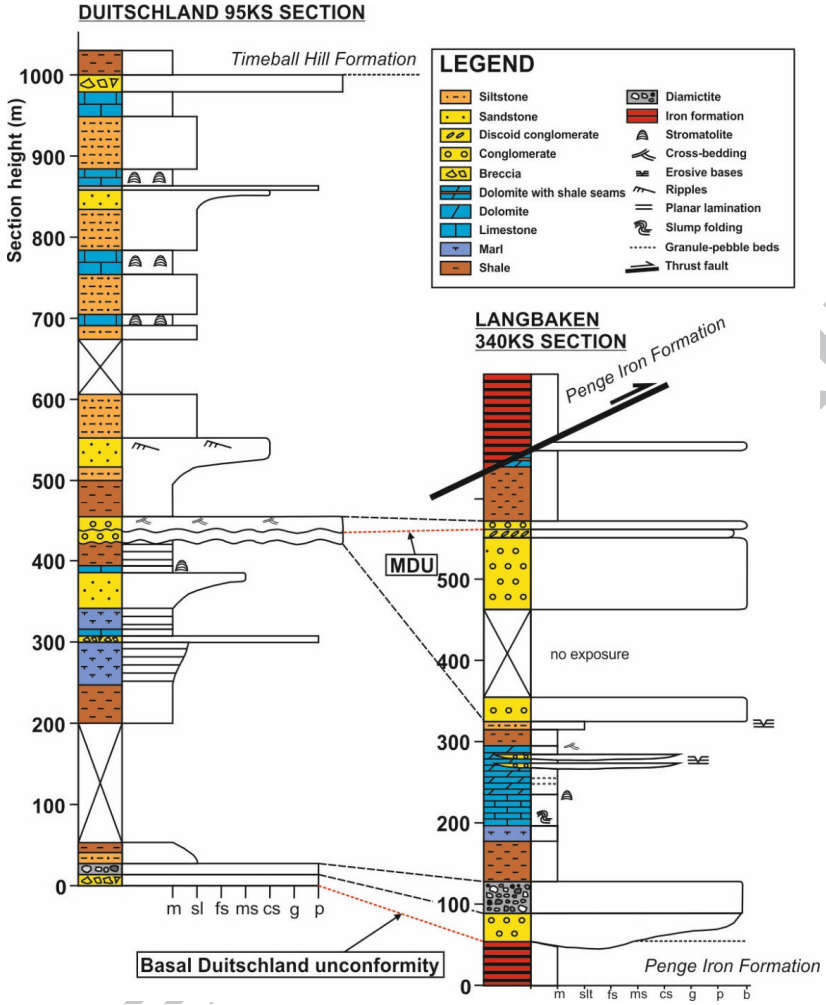

Figure 11: comparison between a schematic log of the Duitschland Formation as typically seen at the type locality of Duitschland 95KS and at other localities and the facies preserved on Langbaken 340KS (log complied from logs shown in Figure 6).

ACCEPTED MANUSCRIPT

chert clasts (up to 15 %), chlorite and biotite, and a matrix with a goethite overprint. Near to the thrust fault some quartz-rich (91 %) samples possess a recrystallized texture with undulose extinction visible. Samples away from the fault, which have not been recrystallized, are typically poorly sorted with no dominant rounding or spherecity type evident. Some samples show minor quartz cements and overgrowths on both quartz and chert grains.

5. Discussion

5.1 Comparison with established Duitschland sections

Previous studies have given sedimentological descriptions from Langbaken limited to sections along the access road (Button, 1973; Coetzee, 2001) or presented geochemical data with no sedimentary profile (Bekker et al., 2001). None of these studies note the two key differences between Langbaken 340KS and Duitschland 95KS type section (Figure 11): (i) the thickness (up to 134 m) and variety of conglomerate facies, and (ii) the angular nature of the MDU. Previous studies of the Duitschland Formation – i.e of sections at Duitschland 95KS, De Hoop 53KS (Figure 2) and regional drill core – have not observed >25 m of conglomerate associated with the MDU (Button, 1973; Bekker et al., 2001; Coetzee, 2001; Buick et al., 1998; Frauenstein et al., 2009). Only Button (1973) mentions an enigmatic “discoid” conglomerate facies; this term is reused for LF6B. Thus, the conglomerates at Langbaken are likely a relatively localized feature, not currently accommodated within any present depositional model of the lower Duitschland Formation. A revised depositional model must explain the observations specific to Langbaken, namely: (i) the upwards progressive development of thicker and wider conglomerate channels in the lower carbonates, (ii) the generation of accommodation space to allow for the accumulation of ~125 m of various conglomeratic facies, (iii) the cause of the southward discoid conglomerate imbrication, and (iv) the angular nature of the MDU.

5.2 Lithofacies interpretation

5.2.1 Deep water, glacial, and carbonate ramp sedimentation

ACCEPTED MANUSCRIPT

The iron formation beds (LF1) exposed to the north of Langbaken 340KS are part of the Penge Iron Formation. Prior to the deposition of the Duitschland Formation uplift and exposure associated with the formation of the basal Duitschland unconformity led to localized reworking of the unit, producing the conglomeratic and brecciation textures observed (Figure 7A and B). In localized areas a basal chert conglomerate (LF6D) marks the beginning of the deposition of the Duitschland Formation. Field and microfacies observations show a strong similarity between this conglomerate and the overlying glacial diamictite. As the conglomerate tends towards a more clast supported nature the two units are separated here, however they may have shared a similar glacial origin. This conglomerate is not interpreted to have formed in a similar manner to the overlying conglomerate lithofacies (LF6A-C) which are discussed below.

The diamictite (LF2) above the conglomerate is indisputably glacial in origin as confirmed by the observation of striated clasts, identified here and in previous studies (Martini, 1979; Coetzee, 2001). The limited range of clast lithologies and the highly ferruginous nature of the matrix suggest it has been mostly derived from the erosion of the underlying Penge Iron Formation. Shales (LF3) which overlie the diamictites result from sedimentation in a low energy, distal setting and show no evidence of glacial influence. Marls (LF4) were also deposited in low energy but slightly more proximal settings and are transitional between shales (LF3) and the lower carbonates (LF5A&B). Lighter bands, which contain higher amounts of carbonate material, could represent periods of increased carbonate production in the overlying water column or pulses of detrital carbonate from more proximal settings whereas clay-rich, dark bands reflect hemipelagic sedimentation.

Planar laminated and non-laminated limestones (LF5A), which overlie the marls, show no evidence for current agitation and have a small detrital component. As such they were probably deposited in a low-energy, sub-wave base environment. Syn-depositional slumping in the limestones (LF5A) reflect a southward dipping palaeoslope as also inferred by others (Coetzee, 2001; Catuneanu and Eriksson, 2002) and may indicate syndepositional tectonic disturbance. Upsection the dolomites (LF5B) increasingly contain coarser detrital clasts in normally graded

ACCEPTED MANUSCRIPT

beds, exhibit cross lamination and domal (probably stromatolitic) lamination, and are incised by conglomeratic bedflows, indicating deposition in a higher energy, wave-influenced, proximal environment. Overall, this suggests a gradually shallowing-upwards succession with no evidence for sudden breaks in slope gradient, such as is observed in the underlying Tongwane Formation platform (Schröder and Warke, 2016). It is therefore likely that deposition occurred on a carbonate ramp with marl and limestone deposition in sub-wave base, outer ramp settings and dolomites in inner ramp settings above fair weather wave base (Read, 1985; Burchette and Wright, 1992). No hummocky cross-stratification or similar indicator of intermediate energy conditions indicative of the mid-ramp were seen.

The dolomites exposed above the MDU (LF5C) are texturally similar to LF5B and also contain admixed chert granules. However, as these dolomites are intercalated with mm-thick calacareous mudstone beds they were likely deposited in a similar, but slightly lower energy setting to that identified for LF5B. This implies that similar depositional environments re-established after the innundation of the MDU. The LF5C carbonates are not equivalent to the shallow-water stromatolitic carbonates seen in the upper Duitschland Formation on Duitschland 95KS (Coetzee, 2001); the upper Duitschland Formation is not preserved on Langbaken 340KS.

5.2.2 The origin of the angular MDU

As discussed above, at other localities the MDU possesses a disconformable geometry, while the middle portions of the Duitschland Formation contains up to four to five times less conglomerate than seen at Langbaken, with no evidence of incision of lower dolomites by conglomerate beds, or conglomerate imbrication. It is conspicuous that all these variations should occur at one locality, and this spatial heterogeneity may suggest that a single, over-arching mechanism is responsible.

There are two possibilities for the generation of the angular MDU: syn- or post-depositional tilting of the lower Duitschland Formation. In the latter case a compressional tectonic event

ACCEPTED MANUSCRIPT

could have tilted lower Duitschland strata and produced the uplift responsible for the gradual shallowing and eventual exposure of the lower strata, and the generation of the MDU. A compressional regime has been proposed for this time interval (Coetzee, 2001), although that study did not predict tilting of Duitschland Formation strata. Other evidence suggests that the Duitschland Formation (and the entire lower Pretoria Group) was deposited under an extensional tectonic regime (Eriksson et al., 1991; 1993; 2011; Catuneanu and Eriksson, 1999; 2002; Eriksson and Catuneanu, 2004). It has also been proposed that MDU is a cryptic glacial surface, produced during a pronounced 'snowball Earth' lowstand (Hoffman, 2013). The presence of a large glacier in the hinterland of the Duitschland basin is not unreasonable given the glacial diamictite at the base of the succession. Hence, despite no direct evidence for glacial influence on the deposition of the remainder of succession, it is possible that the isostatic effect of an ice-sheet to the north may have tilted lower Duitschland strata northward, as observed. However, the severe limitation of both of these basin-scale processes is that they are inconsistent with the disconformable character of the MDU as seen elsewhere.

Alternatively, syn-depositional tilting does not require a basin-scale mechanism and may occur, for example along isolated displacement faults, normal and/or strike-slip, within discrete portions of the basin. Syn-depositional fault movement of this kind could generate highly localized accommodation space for the conglomerates to accumulate in, and also explain the syn-sedimentary slump folds seen in the lower limestones. It would also be in closer agreement with previous work that places the Pretoria Group in an extensional tectonic regime (Eriksson et al., 1991; 1993; 2011; Catuneanu and Eriksson, 1999; 2002; Eriksson and Catuneanu, 2004); isolated displacement faults in the Duitschland Formation may indicate the onset of this period of basin-wide extension.

5.2.3 Conglomerate facies: a wave-influenced, Gilbert type fan-delta?

More recent depositional models of the Duitschland Formation provide no explanation for the deposition of the conglomerate facies (Coetzee, 2001). Older studies suggested that they may represent beach deposits, based on the imbrication observed in the discoid conglomerate

ACCEPTED MANUSCRIPT

(Button, 1973). Any depositional process proposed must be capable of explaning five key characteristics of the conglomerates: (i) their unstratified nature and clast textures, (ii) the thickness of the deposit, (iii) the lenticular and granule-pebble beds, (iv) the imbricated discoid facies, (v) their direct interface with the carbonate ramp.

Coarse-grained conglomerate deposits intercalated with shales, but little silt or sand grade material, suggest a system which alternated between high-energy and low-energy periods. The poorly-sorted and unstratified texture of the conglomerates also suggests a fairly rapid, high-energy and chaotic mode of deposition. Clasts are typically gravel to cobble sized, but larger clasts are more rounded, possibly suggesting a relatively short, but high-energy transportation path. Massive, poorly-sorted, lenticular conglomerates possess erosive bases and as such scoured into the carbonate ramp, but are onlapped by dolomite, suggesting they were deposited

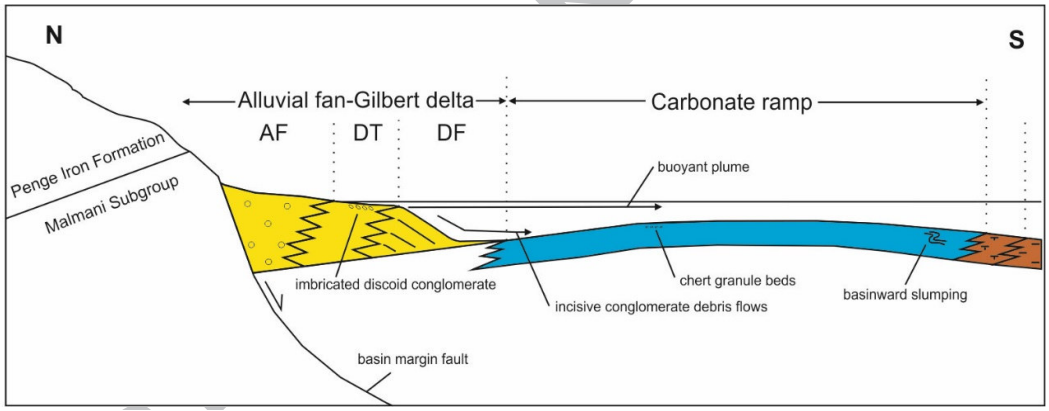

Figure 12: simplified schematic diagram showing all elements of the depositional system at Langbaken 340KS. The basin margin fault is postulated to have a listric geometry so that subsidence causes a northward tilting of the hanging wall block; this would produce the northward dip regime in strata beneath the MDU and would explain the localised angularity of the MDU at Langbaken 340KS. Progressive subsidence causes development of the delta system and its progradation southward. AF = alluvial fan, DT = delta top, DF = delta front. For full description of depositional model see discussion in text and Figure 13. Adapted after Colella (1986) and Massari and Colella (1986).

in discrete, high energy events. It is proposed that an alluvial setting, with an immature Gilbert type-fan delta, prograding onto a carbonate ramp may serve as a suitable depositional model for the lower Duitschland Formation at Langbaken (Figure 12). This setting is consistent with other sections of the lower Duitschland in which deltaic sedimentation has been recognized (Coetzee, 2001).

ACCEPTED MANUSCRIPT

Gilbert-type fan deltas form at the interface between an active alluvial fan and a body of standing water, in either a lacustrine or a marine environment (Nemec and Steel, 1988; Dart et al., 1994; Dorsey et al., 1995; Falk and Dorsey, 1998). They originate as a subaqueous cone of coarse-grained sediment shed from an alluvial fan into the basin (Massari and Colella, 1988). This cone acts as the core of the fan-delta; over time the delta may develop a distinctive tripartite delta architecture divided into distinct subhorizontal topsets and bottomsets separated by a steeply dipping foreset component (Colella, 1988a; Nemec and Steel, 1988; Dart et al., 1994; Dorsey et al., 1995; Mortimer et al., 2005). Fan deltas are progradational systems which commonly, but not exclusively, form in environments where synsedimentary faulting generates accommodation space (Massari and Colella, 1988). Progradation is driven either in response to relative sea-level fall or excessive sediment supply (or both), as long as accommodation space continues to be created, e.g. by synsedimentary subsidence (Colella, 1988b; Kazanci, 1988; McPherson et al., 1988). Slumping of the advancing delta front can cause conglomerates and other delta front facies to be shed as channelized flows into the basin where they are incorporated into the bottomsets (Postma and Roep, 1985; Postma et al., 1988); This processes may be represented by the lenticular conglomerate facies (LF6C).

As the delta continued to advance and evolve, debris flows from the subaerial alluvial fan would have constructed the delta's steep foresets, possibly represented by the massive conglomerate facies (LF6A). Such clinoforms are not observed in LF6A, nor are the normal and inverse grading relationships commonly observed in delta foresets. However, the outcrop at Langbaken approximately runs east-west along the strike of the postulated delta-front (i.e. orthogonal to the southward direction of clinoform progradation) rendering identification of clinoforms difficult. Newly formed or immature Gilbert-deltas, such as considered here, commonly resemble unsorted sediment cones, deposited rapidly where debris flows have been shed from an alluvial fan (Massari and Colella, 1988). This may explain the absence of grading relationships.

The imbricated discoid conglomerate (LF6B) may represent the topset facies, or simply reworking of clasts on the delta-top (Figure 12). On the delta-tops of wave-influenced Gilbert-type fan deltas reworking of facies can often produce a prominent seaward dip of conglomerate

ACCEPTED MANUSCRIPT

clasts, produced by the strong, dominant swash current (Bluck, 1967; Nemec and Steel, 1984; Colella, 1988a; Postma and Cruickshank, 1988; Marzo and Anadón, 1988). Within this model siltstones may represent Gilbert-delta bottomset deposits or silty foreset deposits which have been incised by subsequent conglomeratic foreset forming debris flows (Colella, 1988a). Lithic greywackes and litharenites are also compatible with the Gilbert delta model as sands are found throughout bottomset, foreset and topset facies (Massari and Colella, 1988). Shales interbedded with the conglomerates may represent periods of quiescence and hemipelagic sedimentation (Massari and Colella, 1988; Colella, 1988a; Postma et al., 1988).

The direct interface between a coarse-grained fan delta and a carbonate-dominated depositional environment is unusual, however several analagous Cenozoic systems exist along the margins of the Gulf of Suez, the northern Red Sea, and the Gulf of Aden, and record syn-depositional faulting in an incipient rift setting (Purser and Bosence, 1998). Broadly similar facies assemblages to those described here are seen from mid-Miocene deposits located on the northwestern margin of the Red Sea at Sharm el Behari, where fan-delta deposits pass laterally into marls (Purser et al., 1998). Mid-Miocene syn-rift carbonates deposited on a rotated footwall block in the Gulf of Suez are also noted to interface with fan-deltas during syn-depositional faulting produced by reactivation of boundary faults (Burchette, 1988; James et al., 1988).

Two other depositional settings are possible for the Duitschland Formation: (i) debris flows in an alluvial setting, and (ii) glacial outwash. Setting (i) explains some elements of the facies assemblage such as poor sorting, chaotic deposition, lateral fining, and erosive, lenticular conglomerate beds. This mode of deposition could occur in a tectonically active setting where accommodation space is being generated. However, it requires mechanical wave-reworking to explain the southward imbrication of the discoid conglomerate, at which point this depositional mechanism becomes a coarse grained delta which is not significantly different than what is proposed. In the case of alternative setting (ii), there is no evidence within the conglomerate facies, or in the facies assemblage immediately underlying the conglomerates, to suspect a

ACCEPTED MANUSCRIPT

glacial influence on deposition. The facies assemblage observed is not comparable to Neoproterozoic glacial conglomeratic systems (Busfield and Le Heron, 2016).

In summary, the Gilbert-delta model proposed here, coupled with syn-sedimentary fault subsidence in the Duitschland Basin, is the simplest model as it addresses and accommodates all of the unique observations made at Langbaken and incorporates them in a single, coupled, sedimentary-tectonic model. The model fits with previous contributions which interpret the coarsening upward sequences in the Duitschland Formation as deltaic (Coetzee, 2001). It is also analogous to the fan deltas noted in the lower Rooihoogte Formation (Eriksson, 1988; Catuneanu and Eriksson, 2002; Eriksson and Catuneanu, 2004). This similarity supports the notion that the Rooihoogte Formation is a lateral correlative of the Duitschland Formation (Coetzee, 2001; Luo et al., 2016). Fan deltas are not seen uniformly in the Rooihoogte Formation due to significant lateral heterogeneity in sedimentation patterns and accommodation space across the Transvaal Basin (Eriksson, 1988; Coetzee, 2001; Luo et al., 2016).

ACCEPTED MANUSCRIPT

ACCEPTED MANUSCRIPT

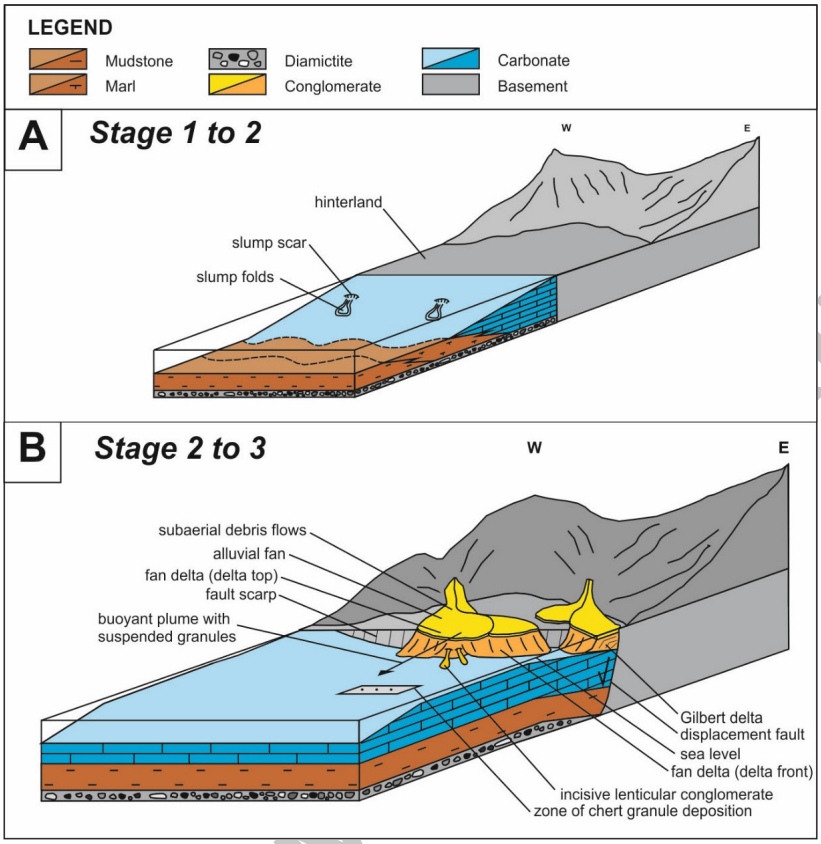

Figure 13: (A) lower portion of the Duitschland Formation: following deposition of the glacial diamictite a carbonate ramp (dip vertically exaggerated) is established which passes basinwards into marl and shale; (B) active faulting along a displacement fault leads to shedding of alluvial fan conglomerates on to the subsiding hanging-wall block to form a Gilbert-type fan delta. The progressive, rotation tilting of the hanging-wall block produces a localised northward dip of bedding and the angular nature of the MDU seen at Langbaken 340KS.

5.3 Depositional Model for the lower Duitschland Formation

5.3.1.Stage 1 – glacial retreat and low energy sedimentation

Drowning of the basal Duitschland unconformity during transgression was followed by the deposition of conglomerates (LF6D) which were shed into limited portions of the basin, incising into the underlying iron-formation and shales of the Penge Iron Formation (LF1). Glacial conditions predominated at this time leading to the deposition of the glacial diamictite (LF2) which drapes the unconformity surface. During post-glacial transgression, low energy, deep water sedimentation began, leading to the deposition of shales (LF3; Figure 13*)*. In the north of the basin, within the study area, carbonate deposition began and a carbonate ramp established.

ACCEPTED MANUSCRIPT

5.3.2 Stage 2 – carbonate ramp and Gilbert-delta progradation

As relative sea-level fell (Coetzee, 2001; Catuneanu and Eriksson, 2002; Eriksson and Catuneanu, 2004), the shallow-water carbonate depositional environments prograded basinwards and the export of carbonate mud from the approaching ramp lead to the deposition of calcareous mudstones (LF4). Limestones (LF5A) were deposited on the outer ramp which possessed a southward dipping palaeoslope while cross-bedded dolomites (LF5B) indicate deposition above wave-base on the inner ramp (Figure 13; Burchette and Wright, 1992).

Continued regression coincided with syn-sedimentary extensional faulting, which produced at least one isolated depocentre within the Duitschland Basin. Conglomerates (LF6A) were shed into this new accommodation space, leading to the creation of a coarse-grained, Gilbert type fan delta at the interface between a carbonate ramp and a progradational alluvial delta system. When sediment supply exceeded the rate of subsidence, or relative sea-level fell sufficiently, the top of the Gilbert delta was reworked by swash currents producing basinward clast imbrication (LF6C). The steepened delta front is susceptile to failure, particularly during seismic disturbances associated with fault movement (Colella, 1988a; McPherson et al., 1988; Postma et al., 1988); these tectonic disturbances may also have caused the slumping observed in more distal carbonate facies. Debris flows triggered during fault movement are shed southward, ahead of the delta front cutting channels into the ramp carbonates (LF6C). Individual coarse clasts, from granule to pebble size, may be carried further out onto the ramp where they are interbedded with carbonate facies (LF5B, LF6C).

5.3.3 Stage 3 – the formation of the MDU

Continued subsidence along a normal (possibly listric) fault would generate accommodation space and also produce the northward (~15 °) tilt of the beds observed below the MDU, when bedding orientations are corrected for later tilting of Pretoria Group strata. Ultimately erosion along the MDU is caused by relative uplift and exposure, most likely due to a relative sea-level

ACCEPTED MANUSCRIPT

lowstand as suggested by the shallowing upward nature of the lower Duitschland Formation (Catuneanu and Eriksson, 1999; 2002; Eriksson and Catuneanu, 2004; Hoffman, 2013). At Langbaken this led to the generation of an angular MDU, whereas elsewhere in the basin a disconformable MDU was generated. In an alternative scenario, it was recently proposed that the MDU represents a 'cryptic glacial unconformity' attributable to a glacio-eustatic sea-level fall produced during a 'snowball Earth' event (Hoffman, 2013). Given the basal Duitschland glacial diamictite, it is not unreasonable to propose that the lowstand associated with the MDU may have been glacial in origin (Hoffman, 2013). Evidence from this contribution has not confirmed that hypothesis; for example no glacial pavements, ice rafted debris, or striated conglomerate clasts were noted despite detailed study of MDU-associated deposits. However, the MDU was produced during a lowstand which may have been a 'normal' glacio-eustatic lowstand (Catuneanu and Eriksson, 1999; 2002; Eriksson and Catuneanu, 2004) as opposed to one caused by a 'snowball Earth' event (Hoffman, 2013).

5.4 Tectonic setting of the lower Duitschland Formation

Fault-controlled deposition in an isolated depocentre, as outlined here, requires normal movement along a disconnected, displacement fault (Leeder et al., 1988; Leeder, 2011). As coarse-grained sediment was most likely sourced from an alluvial fan, and had a relatively short transport path, it is likely that this fault developed close to the hinterland and the basin margin. The creation of isolated deposcentres along small, normal, displacement faults is characteristic of extensional basins in the incipient stages of rifting (Leeder, 2011). Thus, the isolated depocentre at Langbaken may record incipient rift conditions and basin extension thought to control sedimentation patterns during the deposition of lower Pretoria Group (Eriksson et al., 1991; 1993; 2011; Catuneanu and Eriksson, 1999; 2002; Eriksson and Catuneanu, 2004) and not a foreland basin or passive margin (Button 1973; Bekker et al., 2001; Coetzee, 2001).

5.5 Implications for the GOE and global Paleoproterozoic correlations

5.5.1 The correlation of the Duitschland and Rooihoogte formations

ACCEPTED MANUSCRIPT

The MIF-S signal disappears across the MDU, thus signaling a significant step in atmospheric and surface oxidation (Guo et al., 2009) and implying this surface is of key global importance in understanding the timing of the GOE. However, the upper Rooihoogte Formation (western Transvaal Basin) also records the loss of the MIF-S signal at a slightly later period, in a shale-dominated sediment package that has been correlated with the upper Duitschland Formation (Luo et al., 2016). If correct, this suggests that the Duitschland and Rooihoogte formations both independently record a secular change in global sulfur isotope fractionation. As such, it may be possible to use the disappearance of the MIF-S signal as global chemostratigraphic correlation surface (Hoffman, 2013). However, the stratigraphic and sedimentary context of such chemostratigraphic surfaces needs to be tested thoroughly at regional and global scale. In the case of the Transvaal Basin this interpretation is based entirely on the interpretation that the Duitschland and Rooihoogte formations are laterally correlative units.

Orginally, the two formations were not considered to be laterally correlative (SACS, 1980; Eriksson, 1988). However, following a comprehensive drillcore and outcrop study, Coetzee (2001) proposed that the Rooihoogte and Duitschland formations are equivalent successions and correlated the interpreted lower, middle, and upper portions of the two formations (Figure 14).This correlation was based on the equivalent stratigraphic positions of the successions - unconformably overlying the Chuniespoort group and being sharply and conformably overlain by the Timeball Hill Formation – and several similar sequence and lithostratigraphic trends: (i) a basal chert breccia/conglomerate draping and infilling the basal unconformity which is, in turn, overlain by a diamictite, (ii) two coarsening-upward (deltaic) cycles, (iii) mid-formational lowstand and associated conglomerate beds, and (iv) a capping angular chert breccia that is sharply, but conformably, overlain by the Timeball Hill Formation. Later studies have either employed (Bekker et al., 2001; Hannah et al., 2004; Coetzee et al., 2006; Guo et al., 2009; Luo et al., 2016; Schröder et al., 2016) or not employed (Catuneanu and Eriksson, 2002; Rasmussen et al., 2013; Gumsley et al., 2017) this correlation.

ACCEPTED MANUSCRIPT

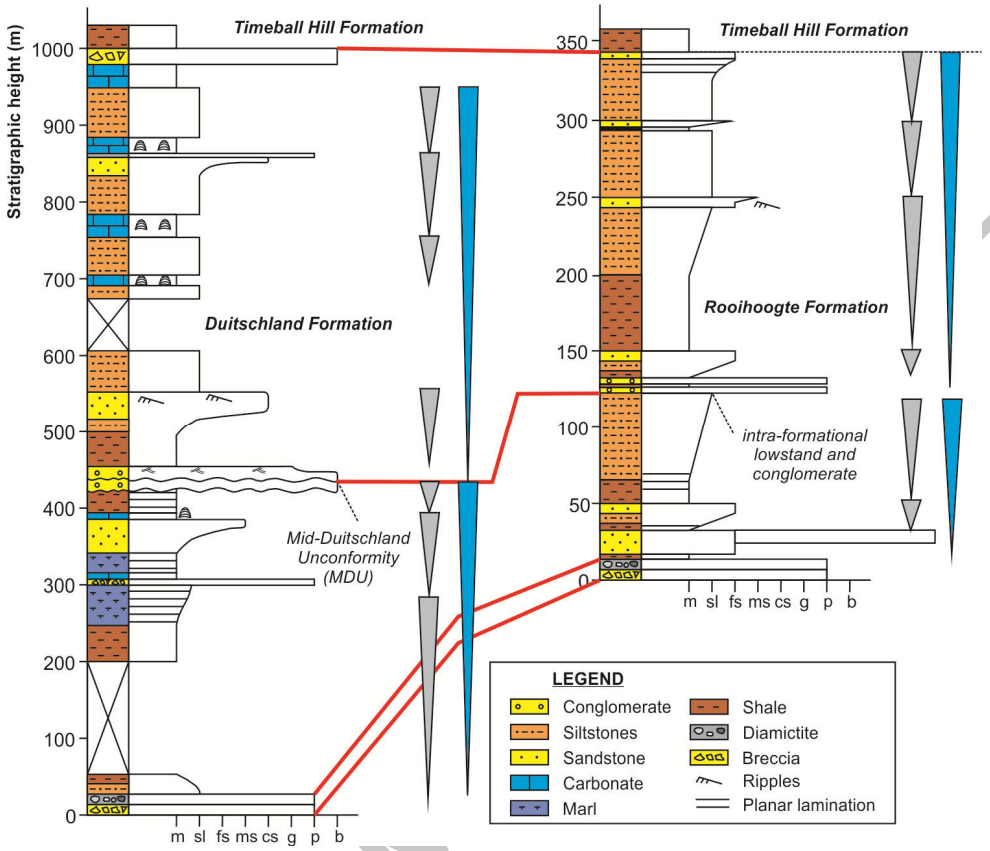

Figure 14: correlation of the Duitschland Formation and the Rooihoogte Formation (at Dwarsberg) as proposed by Coetzee (2001). At Dwarsberg the Rooihoogte Formation has been contact metamorphosed to andalusite grade and is approximately one third the thickness of the Duitschland Formation. The base of both formations consist of conglomerates and diamictites that unconformably overlie the Chuniespoort Group. Both formations consist of coarsening upward, deltaic cycles (grey triangles) that can be grouped into two overall coarsening upward cycles (blue triangles) that are separated by an intraformational unconformity associated with conglomerates. Both successions are sharply overlain by the Timeball Hill formation and record the loss of MIF-S values.

The Rooihoogte Formation displays significant variability in both lithofacies and thickness throughout the western Transvaal Basin. Near Dwarsberg the lithological similarities between the Rooihoogte and Duitschland successions are arguably most clear (Figure 14) despite differing grades of contact metamorphic overprint. Here the Rooihoogte Formation attains a thickness of ~360 m, whereas further south near Potchefstroom this can decrease to <200 m (Coetzee, 2001) and north-west of Johannesburg the formation can be a few tens of meters thick (Eriksson, 1988; Coetzee, 2001). The most notable thickness variations (few 10s of meters to ~100 m) occur within the chert breccia/conglomerate member noted in the lower Rooihoogte

ACCEPTED MANUSCRIPT

Formation (Eriksson, 1988; Coetzee, 2001). These coarse-grained deposits, which occasionally display clast imbrication, have been interpreted as periods of alluvial fan/fan-delta deposition (Eriksson, 1988). Occasionally mudstones contain lenticular conglomerate beds with erosive bases which are interpreted as channel fills (Eriksson, 1988). Similar sedimentological features, or significant lateral lithofacies variability, have not been previously observed in the Duitschland Formation but are noted at Langbaken. Therefore, this contribution adds another line of comparison between the Rooihoogte and Duitschland formations, strengthening their correlation. While it is unlikely that the fan systems in the lower Rooihoogte and mid-Duitschland Formations are directly comparable due to their relative stratigraphic positions, they point towards very similar depositional processes operating in the Transvaal basin at this time.

5.5.2 Oscillations in MIF-S disappearance: real or an artifact?

Recently obtained dates for the Ongeluk Formation volcanics in Griqualand West place their extrusion at 2426 ± 2 Ma, suggesting the entire Postmasburg Group predates deposition of the Pretoria Group, and that the latter has no correlative in Griqualand West (Gumsley et al., 2017). This correlation resolves some long-standing stratigraphic uncertainties in the Transvaal Supergroup, however it also places the Rooihoogte Formation above the Duitschland Formation. As a result, in their discussion of paleoredox proxies preserved in Transvaal strata, these authors need to interpret an oscillating global MIF-S signal to explain the transition from mass-independent to mass-dependent sulfur isotope fractionation observed in both successions. This interpretation would imply a temporal oscillation in sulfur isotope fractionation, reflecting fluctuating concentrations of atmospheric oxygen, thus rendering the end of MIF-S useless as a discrete chemostratigraphic marker. Temporal oscillations between MIF-S and MDF-S conditions may be possible. The precise mechanisms responsible for producing and transferring MIF-S remain unclear (Claire et al., 2014). Further, fluctuations in late Neoarchean MIF-S magnitude that are coupled with organic carbon excursions point towards dynamically oscillating atmospheric compositions that influenced the MIF-S signal recorded in contemporaneously deposited sediments (Farquhar et al. 2007; Zerkle et al., 2012; Izon et al., 2015).

ACCEPTED MANUSCRIPT

However, if the two formations are indeed correlative lateral equivalents - as argued here - then a temporal MIF-S oscillation is not required to explain the observed isotopic trends. Instead, the disappearance of the MIF-S signal can continue to be viewed as a secular, unidirectional change which appears to further support the Duitschland-Rooihoogte correlation. In this scenario it appears that the disappearance the MIF-S can be utilized as a regional, and possibly global, chemostratigraphic correlation surface. This contribution emphasizes the need to consider palaeoredox datasets and interpretations in their stratigraphic and sedimentary framework, and the need to robustly establish such frameworks with detailed sedimentological investigation

5.5.3 The MDU and correlation of Palaeoproterozoic glacials

Another consequence of the new correlation proposed by Gumsley et al. (2017) is that it precludes any correlation of Pretoria Group strata with the Postmasburg Group in Griqualand West. This implies that the Makganyene Formation is older than ~2420 Ma, bringing it into line with the timing of the Huronian glacials as has been previously argued (Bau et al., 1999; Moore et al., 2012; Fairey et al. 2013). While this new correlation does not rule out a causal relationship between the GOE and a a 'snowball Earth' glaciation, it removes arguement that the MDU represents a 'cryptic glacial unconformity' – for which there is no independent sedimentary evidence – that can be correlated with the Makganyene Formation (Hoffman, 2013).

6. Conclusions

The mid-Duitschland unconformity (MDU) separates lower strata of the Duitschland Formation, which retain mass-independently fractionated sulfur isotopes, from the upper portion of the succession where mass-dependently fractionated isotopic signals dominate. Hence, in understanding the evolution of atmospheric oxygen during the GOE the disconformable MDU constitutes a surface of global significance, yet it remains poorly understood. Here, it has been

ACCEPTED MANUSCRIPT

shown for the first time that in parts of the basin the MDU possesses an angular geometry and is associated with significant thicknesses of different conglomerate facies. The lower Duitschland Formation at the locality Langbaken 340KS records interaction of a carbonate ramp with a , wave-influenced, Gilbert-type fan-delta. Deposition was controlled by synsedimentary normal faulting, producing: (i) an isolated deposcentre and accommodation space in which the conglomerates accommodated, (ii) localized tilting of the lower succession, and (iii) synsedimentary slumping in outer ramp limestones. Faulting may have constituted the early stages of extension, and the establishment of the rift setting in which the Pretoria Group was deposited. There is no evidence that the MDU was produced by glacial processes, but it remains possible that the relative sea-level fall associated with its formation may have been glacio-eustatic. The fan-deltas in the Duitschland Formation are analogous to temporal and lateral equivalents in the Rooihoogte Formation, strengthening the lithostratigraphic and chemostratigraphic correlation of the two successions.

7. Acknowledgements

MRW was supported by a NERC-studentship through the University of Manchester. MRW also acknowledges financial support from IAS via a postgraduate grant. SS was supported through a Strategy Grant of the Faculty of Engineering and Physical Sciences at the University of Manchester. J. Waters is thanked for help with the XRD analyses.

8. References

Bau, M., Romer, R.L., Lüders, V. and Beukes, N.J. 1999. Pb, O and C isotopes in silicified Moodraai dolomite (Transvaal Supergroup, South Africa): implications for the composition of Palaeoproterozoic seawater and 'dating' the increase of oxygen in the Precambrian atmosphere. Earth and Planetary Science Letters, 174, 43-57.

Bekker, A., Kaufman, A.J., Karhu, J.A., Beukes, N.J., Swart, Q.D., Coetzee, L.L. and Eriksson, K.A. 2001. Chemostratigraphy of the Paleoproterozoic Duitschland Formation, South Africa: implications for coupled climate change and carbon cycling. American Journal of Science, 301, 261-285.

Bekker, A., Holland, H.D., Wang, P-L, Rumble III, D., Stein, H.J., Hannah, J.L., Coetzee, L.L. and Beukes, N.J. 2004. Dating the rise of atmospheric oxygen. Nature, 427, 117-120.

Bluck, B.J., 1967. Sedimentation of beach gravels: examples from South Wales. Journal of Sedimentary Research, 37, 128-156.

Buick, I.S., Uken, R., Gibson, R.L. and Wallmach, T., 1998. High-δ13C Paleoproterozoic carbonates from the Transvaal Supergroup, South Africa. Geology, 26, 875-878.

ACCEPTED MANUSCRIPT

Burchette, T.P. 1988. Tectonic control on carbonate platform facies distribution and sequence development: Miocene, Gulf of Suez. Sedimentary Geology, 59, 179-204.
Burchette, T.P. and Wright, V.P., 1992. Carbonate ramp depositional systems. Sedimentary Geology, 79, 3-57.
Busfield, M.E. and Le Heron, D.P., 2016. A Neoproterozoic ice advance sequence, Sperry Wash, California. Sedimentology, 63, 307-330.
Button, A. 1973. A study of the stratigraphy and development of the Transvaal Basin in the eastern and northeastern Transvaal. PhD. thesis (unpublished). University of the Witwatersrand, Johannesburg. 133 pp.
Button, A. and Cawthorn, R.G., 2015. Distribution of mafic sills in the Transvaal Supergroup, northeastern South Africa. Journal of the Geological Society, 172, 357-367.
Catuneanu, O. and Eriksson, P.G., 1999. The sequence stratigraphic concept and the Precambrian rock record: an example from the 2.7–2.1 Ga Transvaal Supergroup, Kaapvaal craton. Precambrian Research, 97, 215-251.
Catuneau, O. and Eriksson, P.G., 2002. Sequence stratigraphy of the Precambrian Rooihoogte–Timeball Hill rift succession, Transvaal Basin, South Africa. Sedimentary Geology, 147, 71-88.
Claire, M.W., Kasting, J.F., Domagal-Goldman, S.D., Stüeken, E.E., Buick, R. and Meadows, V.S. 2014. Modeling the signature of sulfur mass-independent fractionation produced in the Archean atmosphere. Geochimica et Cosmochimica Acta, 141, 365-380.
Coetzee, L.L. 2001. Genetic stratigraphy of the Paleoproterozoic Pretoria Group in the western Transvaal. M.Sc thesis (unpublished), University of Johannesburg, 220 pp.
Colella, A. 1988a. Pliocene-Holocene fan deltas and braid deltas in the Crati basin, southern Italy: a consequence of varying tectonic conditions. In: NEMEC, W. and STEEL, R.J. (Eds). Fan Deltas: Sedimentology and Tectonic Settings. Blackie: London, pp 444.
Colella, A., 1988b. Fault-controlled marine Gilbert-type fan deltas. Geology,16, 1031-1034.
Cornell, D.H., Schütte, S.S., and Eglinton, B.L. 1996. The Ongeluk basaltic andesite formation in Griqualand West, South Africa: submarine alteration in a 2222 Ma Proterozoic sea. Precambrian Research, 79, 101-123.
Dart, C.J., Collier, R.E.L., Gawthorpe, R.L., Keller, J.V. and Nicholsl, G. 1994. Sequence stratigraphy of (?) Pliocene-Quaternary synrift, Gilbert-type fan deltas, northern Peloponnesos, Greece. Marine and Petroleum Geology,11, 545-560.
Dorsey, R.J., Umhoefer, P.J. and Renne, P.R. 1995. Rapid subsidence and stacked Gilbert-type fan deltas, Pliocene Loreto Basin, Baja California Sur, Mexico. Sedimentary Geology, 98, 181-204.
Eriksson, P.G. 1988. Sedimentology of the Rooihoogte Formation, Transvaal Sequence. South African Journal of Geology, 91, 477-489.
Eriksson, P.G. and Clendenin, C.W., 1990. A review of the Transvaal Sequence, South Africa. Journal of African Earth Sciences, 10, 101-116.
Eriksson, P.G. and Catuneanu, O., 2004. Third-order sequence stratigraphy in the Palaeoproterozoic Daspoort Formation (Pretoria Group, Transvaal Supergroup), Kaapvaal Craton. In: Eriksson, P.G., Altermann, W., Nelson, D.R., Mueller, W.U. and Catuneanu, O. (eds). The Precambrian Earth: Tempos and Event. Elsevier: Amsterdam, 724-735.
Eriksson, P.G., Schrieber, U.M. and Van der Neut, M., 1991. A review of the sedimentology of the Early Proterozoic Pretoria Group, Transvaal Sequence, South Africa: implications for tectonic setting. Journal of African Earth Sciences, 13, 107-119.
Eriksson, P.G., Schweitzer, J.K., Bosch, P.J.A., Schereiber, U.M., Van Deventer, J.L. and Hatton, C.J., 1993. The Transvaal sequence: an overview. Journal of African Earth Sciences, 16, 25-51.
Eriksson, P.G., Lenhardt, N., Wright, D.T., Mazumber, R. and Bumby, A.J., 2011. Late Neoarchaean-Palaeoproterozoic supracrustal basin-fills of the Kaapvaal craton: Relevance of the supercontinent cycle, the" Great Oxidation Event" and" Snowball Earth"?. Marine and Petroleum Geology, 28, 1385-1401.
Evans, D.A., 2003. A fundamental Precambrian–Phanerozoic shift in earth's glacial style? Tectonophysics, 375, 353-385.
Evans, D.A., Beukes, N.J. and Kirschvink, J.L. 1997. Low-latitude glaciation in the Palaeoproterozoic era. Nature, 386, 262-266.

ACCEPTED MANUSCRIPT

Fairey, B., Tsikos, H., Corfu, F. and Polteau, S. 2013. U-Pb systematics in carbonates of the Postmasburg Group, Transvaal Supergroup, South Africa: Primary versus metasomatic controls. Precambrian Research, 231, 194-205.

Falk, P.D. and Dorsey, R.J., 1998. Rapid development of gravelly high-density turbidity currents in marine Gilbert-type fan deltas, Loreto Basin, Baja California Sur, Mexico. Sedimentology, 45, 331-349.

Farquhar, J., Bao, H. and Thiemens, M. 2000. Atmospheric Influence of Earth's Earliest Sulfur Cycle. Science, 289, 756-758.

Farquhar, J., Peters, M., Johnston, D.T. Strauss, H., Masterson, A., WiechertI, U. and Kaufman, A.M. 2007. Isotopic evidence for Mesoachaean anoxia and changing atmospheric sulphur chemistry. Nature, 449, 706-710.

Frauenstein, F., Veizer, J., Beukes, N., Van Niekerk, H.S. and Coetzee, L.L. 2009. Transvaal Supergroup carbonates: Implications for Paleoproterozoic $\delta^{18}O$ and $\delta^{13}C$ records. Precambrian Research, 175, 149-160.

Gumsley, A.P., Chamberlain, K.R., Bleeker, W., Söderlund, U., de Kock, M.O., Larsson, E.R. and Bekker, A., 2017. Timing and tempo of the Great Oxidation Event. Proceedings of the National Academy of Sciences, 114, 1811-1816.

Guo, Q., Strauss, H., Kaufman, A.J., Schröder, S., Gutzmer, J., Wing, B., Baker, M.A., Bekker, A., Jin, Q. Kim., S-T. and Farquhar, J. 2009. Reconstructing Earth's surface oxidation across the Archean-Proterozoic transition. Geology, 37, 399-402.

Gutzmer, J. and Beukes, N.J., 1998. High-grade manganese ores in the Kalahari manganese field: Characterisation and dating of ore-forming events. Unpublished Report. Rand Afrikaans University, Johannesburg.

Hannah, J.L., Bekker, A., Stein, H.J., Markey, R.J. and Holland, H.D. 2004. Primitive Os and 2316 Ma age for marine shale: implications for Paleoproterozoic glacial events and the rise of atmospheric oxygen. Earth and Planetary Science Letters, 225, 43-52.

Hoffman, P.F. 2013. The Great Oxidation and a Siderian snowball Earth: MIF-S based correlation of Paleoproterozoic glacial epochs. Chemical Geology, 362, 143-156.

Holland, H. D. 2002. Volcanic gases, black smokers, and the Great Oxidation Event. Geochimica et Cosmochicia Acta, 66, 3811-3826.

Holland, H.D. 2006. The oxygenation of the atmosphere and oceans. Philosophical Transactions of the Royal Society B: Biological Sciences, 361, 903-915.

Izon, G., Zerkle, A.L., Zhelezinskaia, I., Farquhar, J., Newton, R.J., Poulton, S.W., Eigenbrode, J.L. and Claire, M.W., 2015. Multiple oscillations in Neoarchaean atmospheric chemistry. Earth and Planetary Science Letters, 431, 264-273.

James, N.P., Coniglio, M., Aissaoui, D.M. and Purser, B.H. 1988. Facies and geologic history of an exposed Miocene rift-margin carbonate platform: Gulf of Suez, Egypt. AAPG Bulletin, 72, 555-572.

Johnson, J.E., Webb, S.M., Thomas, K., Ono, S., Kirschvink, J.L. and FischerI, W.W. 2013. Manganese-oxidising photosynthesis before the rise of cyanobacteria. Proceedings of the National Academy of Sciences of the United States of America, 110, 11238-11243.

Leeder, M., 2011. Sedimentology and Sedimentary Basins: From Turbulence to Tectonics (Second Edition). Wiley-Blackwell: Chichester, 768 pp.

Leeder, M.R., Ord, D.M. and Collier, R. 1988. Development of alluvial fans and fan deltas in neotectonic extensional settings: implications for the interpretation of basin fills. In: NEMEC, W. and STEEL, R.J. (Eds). Fan Deltas: Sedimentology and Tectonic Settings. Blackie: London, pp 444.

Luo, G., Ono, S., Beukes, N.J., Wang, D.T., Xie, S. and Summons, R.E., 2016. Rapid oxygenation of Earth's atmosphere 2.33 billion years ago. Science Advances, 2, p.e1600134.

Lyons, T.W., Reinhard, C.T. and Planavsky, N.J. 2014. The rise of oxygen in Earth's early ocean and atmosphere. Nature, 506, 307-314.

Kazanci, N., 1988. Repetitive deposition of alluvial fan and fan-delta wedges at a fault-controlled margin of the Pleistocene–Holocene Burdur Lake graben, southwestern Anatolia, Turkey. In: NEMEC, W. and STEEL, R.J. (Eds). Fan Deltas: Sedimentology and Tectonic Settings. Blackie: London, pp 444.

Kopp, R.E., Kirschvink, J.L., Hilburn, I.A. and Nash, C.Z. 2005. The Paleoproterozoic snowball Earth: A climate disaster triggered by the evolution of oxygenic photosynthesis. Proceedings of the National Academy of Sciences, 102, 11131-11136.

ACCEPTED MANUSCRIPT

Martini, J.E.J. 1979. A copper-bearing bed in the Pretoria Group in the northeastern Transvaal. Geological Society of South Africa, Special Publication, 6, 65-72.

Marzo, M. and Anadon, P. 1988. Anatomy of a conglomeratic fan-delta complex: the Eocene Montserrat Conglomerate, Ebro Basin, northeastern Spain. In: Nemec, W. and Steel, R.J. (Eds). Fan Deltas: Sedimentology and Tectonic Settings. Blackie: London, pp 444.

Massari, F. and Collela, A. 1988. Evolution and types of fan deltas in some major tectonic settings. In: Nemec, W. and Steel, R.J. (Eds). Fan Deltas: Sedimentology and Tectonic Settings. Blackie: London, pp 444.

McCourt, S., 1995. The crustal architecture of the Kaapvaal crustal block South Africa, between 3.5 and 2.0 Ga. Mineralium Deposita, 30, 89-97.

McPherson, J.G., Shanmugan, G. and Moiola, R.J. 1988. Fan deltas and braid deltas: conceptual problems. In: Nemec, W. and Steel, R.J. (Eds). Fan Deltas: Sedimentology and Tectonic Settings. Blackie: London, pp 444.

Moore, J.M., Polteau, S., Armstrong, R.A., Corfu, F. and Tsikos, H. 2012. The age and correlation of the Postmasburg Group, southern Africa: Constraints from detrital zircon grains. Journal of African Earth Sciences, 64, 9-19.

Mortimer, E., Gupta, S. and Cowie, P., 2005. Clinoform nucleation and growth in coarse-grained deltas, Loreto basin, Baja California Sur, Mexico: a response to episodic accelerations in fault displacement. Basin Research, 17, 337-359.

Nelson, D.R., Trendall, A.F. and ALTERMANN, W. 1999. Chronological correlations between the Pilbara and Kaapvaal cratons. Precambrian Research, 97, 165-189.

Nemec, W. and Steel, R.J. 1984. Alluvial and coastal conglomerates: their significant features and some comments on gravelly mass-flow deposits. In: Koster, E.H.. and Steel, R.J. (Eds). Sedimentology of Gravels and Conglomerates, Canadian Society of Petroleum Geologists, 10, 1-31.

Nemec, W. and Steel, R.J. 1988. What is a fan delta and how do we recognize it? In: Nemec, W. and Steel, R.J. (Eds). Fan Deltas: Sedimentology and Tectonic Settings. Blackie: London, pp 444.

Papineau, D., Mojzsis, S.J. and Schmitt, A.K., 2007. Multiple sulfur isotopes from Paleoproterozoic Huronian interglacial sediments and the rise of atmospheric oxygen. Earth and Planetary Science Letters, 255, 188-212.

Pavlov, A.A. and Kasting, J.F. 2002. Mass-Independent Fractionation of Sulfur Isotopes in Archean Sediments: Strong Evidence for an Anoxic Archean Atmosphere. Astrobiology, 2, 27-41.

Postma, G. and Roep, T.B. 1985. Resedimented conglomerates in the bottomsets of Gilbert-type gravel deltas. Journal of Sedimentary Research, 55, 874-885.

Postma, G. and Cruickshank, C. 1988. Sedimentology of a Weichselian to Holocene terraced fan delta, Varangerfjord, northern Norway. In: Nemec, W. and Steel, R.J. (Eds). Fan Deltas: Sedimentology and Tectonic Settings. Blackie: London, pp 444.

Postma, G., Babaić, L., Zupanič, J. and Røe, S.L. 1988. Delta front failure and associated bottomset deformationin a marine, gravelly Gilbert-type fan delta. In: Nemec, W. and Steel, R.J. (Eds). Fan Deltas: Sedimentology and Tectonic Settings. Blackie: London, pp 444.

Prior, D.B. and Bornhold, B.D. 1988. Submarine morphology and processes of fjord fan deltas and related high gradient systems: modern examples from British Columbia. In: Nemec, W. and Steel, R.J. (Eds). Fan Deltas: Sedimentology and Tectonic Settings. Blackie: London, pp 444.

Purser, B.H. and Bosence, D.W.J., 1998. Organization and scientific contributions in sedimentation and tectonics of rift basins: Red Sea-Gulf of Aden. In: Purser, B.H. and Boscence, D.W.J. (Eds) Sedimentation and Tectonics in Rift Basins: Red Sea – Gulf of Aden. Chapman and Hall, London, 663 pp.

Purser, B.H., Barrier, P., Montenat, C., Orszag-Sperber, F., D'Estevou, P.O., Plaziat, J.C. and Philobbos, E. 1998. Carbonate and siliciclastic sedimentation in an active tectonic setting: Miocene of the north-western Red Sea rift, Egypt. In: Purser, B.H. and Boscence, D.W.J. (Eds) Sedimentation and Tectonics in Rift Basins: Red Sea – Gulf of Aden. Chapman and Hall, London, 663 pp.

Rasmussen, B., Bekker, A and Fletcher, I.R. 2013. Correlation of Palaeoproterozoic glaciations based on U-Pb zircon ages for tuff beds in the Transvaal and Huronian Supergroups. Earth and Planetary Science Letters, 382, 173-180.

Read, J.F. 1985. Carbonate platform facies models. AAPG bulletin, 69,1-21.

ACCEPTED MANUSCRIPT

Reinhard, C.T., Planavsky, N.J. and Lyons, T.W. 2013. Long-term sedimentary recycling of rare sulphur isotope anomalies. Nature, 497, 100-103.

South African Committee for Stratigraphy (SACS). 1980. Stratigraphy of South Africa, Part 1 (Comp L.E. Kent). Lithostratigraphy of the Republic of South Africa, South West Africa/Namibia, and the Republics of Bophuthatswana, Transkei and Venda. Handbook Geological Survey of South Africa, 8, 690 pp.

Schröder, S. and Warke, M.R. 2016. Termination of BIF deposition in the Paleoproterozoic: the Tongwane Formation, South Africa. South African Journal of Geology, 119, 329-346.

Schröder, S., Beukes, N.J. and Armstrong, R.A. 2016. Detrital zircon constraints on the tectonostratigraphy of the Paleoproterozoic Pretoria Group, South Africa. Precambrian Research, 278, 362-393.

Tucker, M.E. 2003. Sedimentary rocks in the field. John Wiley & Sons: Chichester, 234 pp.

Zerkle, A.L., Claire, M.W., Domagal-Goldman, S.D., Farquhar, J. and Poulton, S.W. 2012. A bistable organic-rich atmosphere on the Neoarchaean Earth. Nature Geoscience, 5, 359.

ACCEPTED MANUSCRIPT

ACCEPTED MANUSCRIPT

Highlights

- Field investigation reveals new conglomerate facies in lower Duitschland Formation.
- Intraformational unconformity, associated with loss of MIF-S signal, is angular.
- Syndepositional faulting generated accommodation space infilled by fan deltas.
- New sedimentary observations support correlation with Rooihoogte Formation.
- Suggests recently proposed MIF-S ‘oscillations’ result from incorrect correlation.

ACCEPTED MANUSCRIPT